AGU PUBLICATIONS

JGR

Journal of Geophysical Research: Oceans

RESEARCH ARTICLE

10.1002/2016JC011759

Key Points:
- Time series measurements (2004–2014) of ^{129}I and CFC-11 in DSOW in DWBC on Line W were compared to upstream values in DSOW in Labrador Sea
- Model simulations of tracer levels in the boundary current were used to determine parameters governing advection and mixing
- DSOW is transported to Line W with a flow velocity of 2.7 cm/s and mixing between core and interior occurs with a time constant of 2.6 years

Correspondence to:
J. N. Smith,
john.smith@dfo-mpo.gc.ca

Citation:
Smith, J. N., W. M. Smethie Jr., I. Yashayev, R. Curry, and K. Azetsu-Scott (2016), Time series measurements of transient tracers and tracer-derived transport in the Deep Western Boundary Current between the Labrador Sea and the subtropical Atlantic Ocean at Line W, *J. Geophys. Res. Oceans*, *121*, 8115–8138, doi:10.1002/2016JC011759.

Received 8 MAR 2016
Accepted 1 OCT 2016
Accepted article online 5 OCT 2016
Published online 10 NOV 2016

Time series measurements of transient tracers and tracer-derived transport in the Deep Western Boundary Current between the Labrador Sea and the subtropical Atlantic Ocean at Line W

John N. Smith[1], William M. Smethie Jr.[2], Igor Yashayev[1], Ruth Curry[3], and Kumiko Azetsu-Scott[1]

[1]Bedford Institute of Oceanography, Dartmouth, Nova Scotia, Canada, [2]Lamont-Doherty Earth Observatory of Columbia University, Palisades, New York, USA, [3]Woods Hole Oceanographic Institution, Woods Hole, Massachusetts, USA

Abstract Time series measurements of the nuclear fuel reprocessing tracer ^{129}I and the gas ventilation tracer CFC-11 were undertaken on the AR7W section in the Labrador Sea (1997–2014) and on Line W (2004–2014), located over the US continental slope off Cape Cod, to determine advection and mixing time scales for the transport of Denmark Strait Overflow Water (DSOW) within the Deep Western Boundary Current (DWBC). Tracer measurements were also conducted in 2010 over the continental rise southeast of Bermuda to intercept the equatorward flow of DSOW by interior pathways. The Labrador Sea tracer and hydrographic time series data were used as input functions in a boundary current model that employs transit time distributions to simulate the effects of mixing and advection on downstream tracer distributions. Model simulations of tracer levels in the boundary current core and adjacent interior (shoulder) region with which mixing occurs were compared with the Line W time series measurements to determine boundary current model parameters. These results indicate that DSOW is transported from the Labrador Sea to Line W via the DWBC on a time scale of 5–6 years corresponding to a mean flow velocity of 2.7 cm/s while mixing between the core and interior regions occurs with a time constant of 2.6 years. A tracer section over the southern flank of the Bermuda rise indicates that the flow of DSOW that separated from the DWBC had undergone transport through interior pathways on a time scale of 9 years with a mixing time constant of 4 years.

1. Introduction

An important control on climate is the global meridional overturning circulation (MOC) whose intensity appears to be related to climate change on decadal or greater time scales [*Curry et al.*, 1998; *IPCC*, 2014]. The MOC involves the near-surface transport of warm waters poleward to high latitudes where they cool, sink, and spread equatorward through multiple pathways into the deep interior oceanic basins. *Stommel* [1958] originally noted the theoretical importance of western intensified boundary currents in the deep southward flow of recently ventilated water from higher latitudes. It was generally thought that the most important pathway in the North Atlantic was the Deep Western Boundary Current (DWBC) which originates in the Nordic and Labrador Seas, flows southward along the North American continental slope, and exchanges water with the ocean interior (Figure 1). More recent work reflects on the comparative importance of interior pathways that can provide additional routes for advection of polar and subpolar waters to the subtropics. An accurate understanding of transport rates in the DWBC and along interior pathways is important in determining the propagation of heat, anthropogenic carbon, and high-latitude climate signals from the subpolar to subtropical gyres and evaluating how intermediate and deep water anomalies may affect mid and low-latitude circulation patterns.

Time scales for transport in the North Atlantic DWBC have been inferred using a variety of techniques including measurements of temperature and salinity anomalies, tracers, direct current measurements, and neutral buoyancy floats. Some of these methods have given sharply divergent results. For example, mean velocities of 5–10 cm/s have been measured in the DWBC using current meters [e.g., *Watts*, 1991; *Pickart and Smethie*, 1998; *Toole et al.*, 2011], whereas spreading rates of 2–2.5 cm/s have been inferred from the

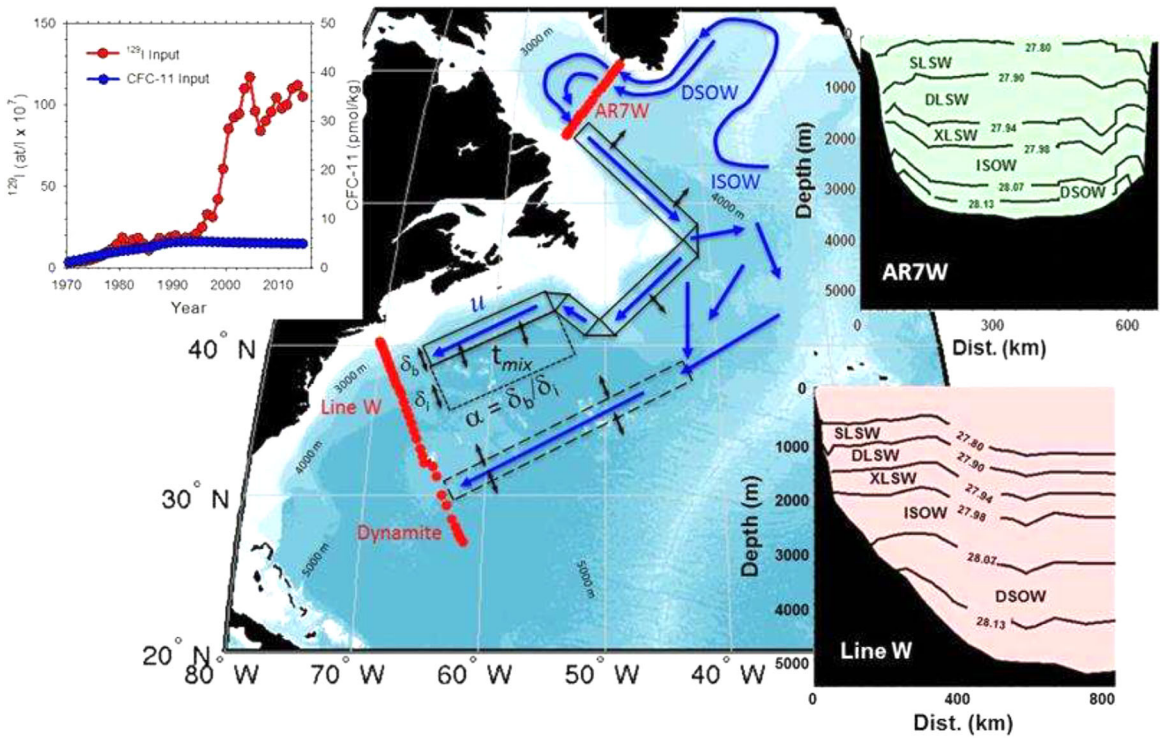

Figure 1. DSOW flows southwestward from Denmark Strait with ISOW, crosses Line AR7W in the Labrador Sea and then flows southward in the DWBC along the 3500–4000 m isobath of the North American continental slope past Line W. DSOW also separates from the slope and follows interior pathways across the Dynamite Line to the subtropical gyre. Boundary current model is illustrated by rectangles and described in the text where u is the flow velocity, t_{mix} is the mixing constant, α is the ratio of the widths of the core (δ_b) to interior regions (δ_i) of the boundary current. Top left inset: Input functions for CFC-11 and ^{129}I for DSOW in Denmark Strait. Top right inset: Water mass classifications on AR7W Line defined by neutral density limits (γ^n). Bottom right inset: Water mass classifications on Line W.

propagation of hydrographic anomalies [e.g., *Molinari et al*., 1998; *Freudenthal and Andrie*, 2002; *Steinfeldt et al*., 2007], and values of only 1–2.5 cm/s estimated from transient tracer studies [e.g., *Doney and Jenkins*, 1994; *Smethie et al*., 2000; *Fine et al*., 2002; *Rhein et al*., 2015]. These discrepancies generally stem from the fact that each method tends to measure different properties of the flow field on different time scales.

The importance of alternate pathways to the DWBC for equatorward transport of high-latitude water was illustrated by *Bower et al*. [2009, 2011] who used isobaric floats to follow the diversion of the flow of Labrador Sea Water (LSW) from bathymetric "choke" points such as Flemish Cap and the Tail of the Grand Banks through the interior basin, while modeling exercises [*Zhang*, 2010; *Gary et al*., 2011] have provided support for the importance of these interior pathways. *van Sebille et al*. [2011] also emphasized the significance of interior pathways in their comparison of salinity time series on the Abaco Line at 26°N with Labrador Sea time series and estimated a mean equatorward flow velocity of 2.5 cm/s for LSW, in agreement with earlier studies by *Molinari et al*. [1998]. *Lozier et al*. [2013] extended the above studies of LSW to the overflow waters (OW) using an ocean general circulation model and also noted the relatively large amount of equatorward flow of OW by interior pathways rather than in the DWBC.

One of the confounding factors in evaluating transport time scales both in the DWBC and on interior pathways is accounting for recirculation [*van Sebille et al*., 2011]. Recirculation not only increases the path length and thereby lengthens the time scale for the flow of discrete volume elements of water, but it also introduces mixing between water parcels labeled by interannual components of the tracer input functions. One method for evaluating the effects of recirculation on the spreading rates of tracers focuses on boundary current models that can be used to estimate the current velocity of the boundary flow between the point of tracer input and point of observation and simultaneously determine mass exchange rates between the core and interior waters. This type of study is best suited to transient tracers whose input functions vary on time scales similar to those that characterize mixing in the boundary current [*Waugh and Hall*, 2005]. In addition to hydrographic tracers, we employ a ventilation tracer CFC-11 that is delivered to the ocean from the

atmosphere and a long-lived ($t_{1/2}$ = 16 million years) radioactive tracer ^{129}I that is discharged directly into coastal waters from European nuclear fuel reprocessing plants. This tracer combination provides a signal that varies comparatively rapidly on decadal time scales. In contrast to previous studies in the DWBC [*Doney and Jenkins*, 1994; *Pickart and Smethie*, 1998; *Waugh and Hall*, 2005] which have relied on tracer input functions estimated from atmospheric concentrations and tracer data collected along the axis of flow, the present work focuses on tracer time series comparisons. The tracer input functions for the DWBC and specifically the DSOW component of the DWBC have been measured directly by annual occupations of an upstream section (AR7W Line) in the Labrador Sea (Figure 1). The direct measurement of the time varying, tracer input functions in DSOW in the Labrador Sea eliminates issues associated with uncertainties in tracer input functions for atmospheric or nuclear fuel reprocessing plant sources or with uncertainties associated with mixing during tracer transport from these sources to the Labrador Sea. Downstream tracer measurements were conducted both on Line W, a section across the US continental slope south of Cape Cod and on the "Dynamite Line" stretching southeastward over the Bermuda Rise (Figure 1). These results are incorporated into the boundary current model of *Waugh and Hall* [2005] to estimate advection time scales and mixing rates for flow within the DWBC and along ocean interior pathways.

2. Model and Analytical Methodology

2.1. Boundary Current Model

The purpose of a boundary current model is to simulate transport in the boundary current in a manner that invokes water mass mixing as well as advection. A relatively simple kinematic boundary current model has been formulated by *Waugh and Hall* [2005] that can be applied to tracer transport in the DWBC. Although this model is similar to the numerical models developed by *Doney and Jenkins* [1994] and *Pickart et al.* [1989], it has the advantage that the transport properties of interest (advection and mixing rates) are parameterized and can be varied independently. The model is based on the idea that the dominant mixing in the DWBC occurs laterally between the boundary current and the interior region rather than in the direction of flow. The boundary current is represented as a one-dimensional, advective-diffusive region that exchanges water and tracers with a much more slowly moving, adjacent interior shoulder region as illustrated in Figure 1. The ratio of the width of the boundary current δ_b to the width of the interior shoulder region, δ_i is given by the parameter, α ($=\delta_b/\delta_i$; Figure 1). Mass exchange between the boundary current and the interior region is characterized by a mixing time constant, t_{mix}.

Waugh and Hall [2005] made the additional simplifying assumptions that along-flow diffusion in the boundary current is negligible compared to lateral mixing and that motion in the interior shoulder region can be neglected. These assumptions can be justified using scaling arguments and through comparison of the boundary current model results with numerical models [*Waugh and Hall*, 2005]. Using these assumptions, the tracer continuity equations for the DWBC model are

$$\frac{\partial \chi_b}{\partial t} + u\frac{\partial \chi_b}{\partial x} + \frac{1}{t_{mix}}(\chi_b - \chi_i) = S, \tag{1}$$

$$\frac{\partial \chi_i}{\partial t} - \frac{\alpha}{t_{mix}}(\chi_b - \chi_i) = S, \tag{2}$$

where x is distance along the direction of flow, subscripts b and i refer to quantities in the boundary current and interior region, respectively, χ (x, t) is the tracer concentration, u is the flow velocity in the x direction, and S (x, t) is the tracer source or sink term.

Previous studies have applied similar equations to estimate boundary current flow using numerical methods [*Doney and Jenkins*, 1994; *Pickart et al.*, 1989; *Rhein*, 1994; *Haine et al.*, 1998]. However, recent studies have tended to focus on the formulation of transit time distributions (TTD) which reflect the observation that there is no single time for transport of a property from one location to another, but rather a distribution of transit times. The TTD can be used to represent the propagation of a boundary condition on a tracer concentration (given by the known tracer input function) to a downstream location. For example, the concentration of a passive tracer, χ (x, t) at a location, x and time, t is given by

$$\chi(x,t)=\int_0^\infty \chi(0,t-t')G(x,t')dt', \tag{3}$$

where $G(x,t)$ is the TTD and χ (0, t) is the tracer input function at $x=0$. In order to apply this technique, it is necessary to know the TTD at each location in the model regime and the tracer input function. *Waugh and Hall* [2005] addressed this problem by solving equations (1) and (2) for the TTDs, $G_b(x,t)$, and $G_i(x,t)$ with $S_b=S_i=0$ and the boundary condition $\chi_b(0,t)=\delta(t)$ giving

$$G_b(x,t)=\hat{G}_1\delta(t-t_{adv})+\hat{G}_2\theta(t-t_{adv}), \tag{4}$$

$$G_i(x,t)=\hat{G}_3\theta(t-t_{adv}), \tag{5}$$

where

$$\hat{G}_1=e^{-t_{adv}/t_{mix}},\ \hat{G}_2=\frac{\alpha}{\zeta t_{mix}}e^{-(1+\zeta^2)t_{adv}/t_{mix}}I_1(2\zeta t_{adv}/t_{mix}), \tag{6}$$

$$\hat{G}_3=\frac{\alpha}{t_{mix}}e^{-(1+\zeta^2)t_{adv}/t_{mix}}I_0(2\zeta t_{adv}/t_{mix}), \tag{7}$$

t_{adv} is the advective time to reach position, x ($=x^\circ/u$, where x° is the distance, 4600 km between the midpoint of the AR7W section and Line W), $\zeta^2=(\alpha u/x)(t-x/u)$, I_0 and I_1 are the modified Bessel functions of zeroth and first order, δ is the Dirac delta function, and θ is the Heaviside function. Equation (3) can then be used to calculate downstream tracer concentrations in the boundary current core and interior shoulder region using $G_b(x,t)$ and $G_i(x,t)$, respectively, for a given upstream tracer input function. Previous studies in the DWBC have used tracer input functions estimated indirectly from atmospheric input functions. In the present study the upstream tracer input functions are determined empirically from tracer time series measurements in the Labrador Sea and the only unknowns in the boundary current model are the parameters, α, t_{mix}, and t_{adv}.

2.2. Analytical Methods

One liter PVC bottles were filled with seawater from 10 L Niskin bottles deployed at stations along the AR7W transect (WOCE repeat line) in the Labrador Sea and on Line W off Cape Cod (Figure 1). The AR7W line has been sampled annually by DFO since 1993 as part of its ongoing Atlantic Zone Off-shelf Monitoring Program (AZMP) [*Greenan et al*., 2010] and Line W was sampled semiannually for tracers from 2004 to 2008 and annually thereafter to 2014. Samples were also collected during the 2010 cruise of the Atlantic Explorer on a southeast transect from Bermuda over the Bermuda Rise as part of the WHOI Dynamite program. ^{129}I analyses were performed on the 1 L samples by accelerator mass spectrometry [*Kilius et al*., 1992, 1994; *Smith et al*., 1998] at the IsoTrace Laboratory at the University of Toronto. The sample data were normalized to IsoTrace Reference Material #2 (^{129}I/^{127}I = 1.174 $\times$ 10^{-11} atom ratio). The blank (KI carrier added to distilled water) for this procedure is 0.75 $\pm$ 0.10 $\times$ 10^7 atoms/L and the standard deviation (one sigma) ranged from 5 to 10% [*Edmonds et al*., 1998].

Water samples for CFC measurements were collected from the same sampling bottles on the rosette used for the ^{129}I measurements. For the Labrador Sea samples, water was drawn into 100 mL glass syringes and sealed with stainless steel Luer caps. Samples were stored submerged in a bath of running seawater prior to analysis. An automated purge and trap system was used to strip halogenated carbon compounds (halogens) from seawater. A measured volume of seawater (ca. 25 mL) was passed to a purge chamber, warmed to 20°C, and purged with UHP Nitrogen. The analytes were then trapped on a chromatographic absorbent, packed in stainless steel tubing, and then desorbed by heating the trap to 170°C. The halogens were separated using gas chromatography. An electron capture detector was employed for halogen analyses, which was operated at a temperature of 350°C using UHP Nitrogen as a carrier gas [*Azetsu-Scott et al*., 2003, 2005]. A similar procedure was used for the Line W CFC measurements. For these samples, a standard prepared by J. Bullister for the Repeat Hydrography lines run between 2002 and 2008 was used and the results are reported on the SIO98 scale. The precision for CFC-11 measurements for both regions was generally $\pm$1% or better.

3. Results

3.1. ^{129}I and CFC-11 Transport Pathways

Radioactive tracers discharged from the La Hague, France and Sellafield, UK nuclear fuel reprocessing plants into the English Channel and Irish Sea, respectively, are transported through the North Sea and into the Norwegian Atlantic Current flowing northward toward Fram Strait [*Smith et al*., 2005]. Approaching Fram Strait, the Atlantic Water (AW) flow bifurcates with the eastern branch flowing into the Arctic Ocean and the western branch undergoing recirculation and joining the southward flowing East Greenland Current (EGC) as Return Atlantic Water (RAW) [*Fogelqvist et al*., 2003]. The EGC flows southward through Denmark Strait in two bifurcated branches with deeper components, including modified Atlantic Water, RAW, and inputs from the North Icelandic Jet contributing to the DSOW that descends to the bottom of the Irminger Sea [*Swift et al*., 1980; *Rudels et al*., 1999; *Våge et al*., 2011, 2013]. In the Irminger Sea basin DSOW is overridden by Iceland Scotland Overflow Water (ISOW) that has entered the basin from the eastern North Atlantic through the Charlie-Gibbs Fracture Zone as the two water masses flow cyclonically around the basin and into the Labrador Sea (Figure 1) [*Swift*, 1984].

The deep overflow waters enter the Labrador Sea as a boundary current that broadens as it spreads across the gently sloping bathymetry of the basin as a relatively weakly stratified, water mass characterized by low potential vorticity (PV) [*Yashayaev and Dickson*, 2008; *Xu et al*., 2015]. DSOW exits the Labrador Sea approximately 0.5–1 year later [*Smith et al*., 2005] as a narrow flow southward along the 3000–3500 m isobath of the Newfoundland continental slope [*Fischer et al*., 2004] and enters the Newfoundland Basin as part of the lower limb of the DWBC. DSOW encounters multiple cyclonic recirculation cells in the Newfoundland basin driven mainly by the upper layer influence of the strong North Atlantic Current with topographic blocking and eddy variability near Flemish Cap also playing a role [*Xu et al*., 2015]. The densest component enters the recirculation cells and a less dense mixture of DSOW and ISOW flows southward around the tail of the Grand Banks with DSOW contributing the bulk of the anthropogenic tracer signal [*Smethie et al*., 2000].

According to the traditional model [*Stommel*, 1958], the flow of DSOW south of the Newfoundland Basin is contained within the lower limb of the DWBC which itself has been assumed to be the principal conduit for the equatorward transport of newly ventilated water from high latitudes. This model predicts that the downstream configuration of the DSOW plume can then be evaluated by studying its flow across Line W (Figure 1) over the US continental slope. One small drifter study has been conducted in the DSOW/ISOW component of the DWBC, which showed that the flow bifurcated when it crossed beneath the Gulf Stream with one path extending equatorward along the western boundary and one extending eastward in the direction of the Gulf Stream before turning southward [*Bower and Hunt*, 2000a, b]. More extensive observational and model drifter studies for the overlying Labrador Sea Water (LSW) component of the DWBC have been reported by *Bower et al*. [2009, 2011]. They have shown separation of the boundary current from the slope during flow over the bathymetric curvature at the tail of the Grand Banks resulting in the development of alternate interior southward flow pathways through the Atlantic basin. Interaction of the DWBC with the deep recirculations in the subtropical gyre causes sufficient transport away from the boundary so that the subsequent southward transport through the basin interior is similar in magnitude to equatorward flow in the narrow, constrained DWBC [*Gary et al*., 2011]. *Lozier et al*. [2013] applied an ocean general circulation model to similar studies of the Overflow Water (OW) and observed that these water masses also undergo significant equatorward flow through interior pathways in the model simulations.

3.2. ^{129}I and CFC-11 Input Functions

The ^{129}I input function for DSOW at Denmark Strait (Figure 1, inset) was calculated using an empirically determined, transfer factor (TF) of 0.67×10^{-12} μmol L^{-1}/mol yr^{-1} and transit times of 5 yr from La Hague and 7 yr from Sellafield [*Smith et al*., 2005]. The tracer signal from the reprocessing sources is superimposed on a small ^{129}I fallout background for Atlantic water (2.5×10^7 atoms/L) [*Smith et al*., 1998, 1999, 2005, 2011; *Edmonds et al*., 2001]. The input function for CFC-11 for DSOW (75% saturation) has been estimated by *LeBel et al*. [2008] and is compared to that for ^{129}I in Figure 1 (inset). Input functions for ^{129}I and CFC-11 have also been estimated for ISOW [*Smethie and Fine*, 2001; *Smith et al*., 2005; *LeBel et al*., 2008]. Tracer levels in ISOW are lower than those in DSOW, because ISOW has both a longer ventilation time within the Nordic Seas and a longer pathway to the Irminger Sea [*Smethie and Swift*, 1989; *Smethie*, 1993]. Until 1994 the input functions of ^{129}I and CFC-11 varied approximately proportionally, but beginning in 1994 the input function

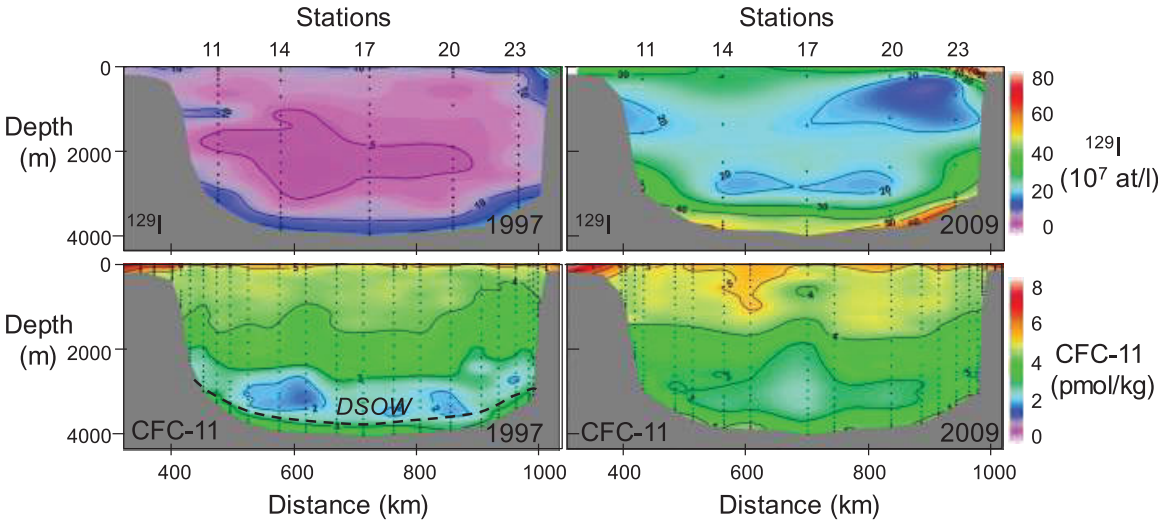

Figure 2. (left) Labrador Sea AR7W Line sections for ^{129}I and CFC-11 for 1997. (right) AR7W Line sections for ^{129}I and CFC-11 for 2009. The large increase in ^{129}I levels in all Labrador Sea water masses by 2009 reflects the rapid increase in the ^{129}I input function in the 1990s (Figure 1). The ^{129}I increase is particularly pronounced in DSOW which has the most direct connection with the Nordic Seas and which is defined by the 28.13 neutral density surface located about 100 m from the bottom (dashed line, bottom left).

for ^{129}I increased relative to CFC-11 owing to enhanced rates in reprocessing plant discharges. This has resulted in a time varying change in the relative ^{129}I and CFC-11 concentrations in formation regions for DSOW, thereby providing the structure for a dual tracer experiment for measuring transit times and ventilation ages of water masses entering the deep North Atlantic.

3.3. Labrador Sea Results

The water masses in the Labrador Sea can be defined by the neutral density boundaries given schematically in Figure 1 (inset). The three classes of LSW [shallow (SLSW), deep (DLSW), and extreme (XLSW)] extend from about 150 to 2200 m. They are well ventilated due to interaction with the atmosphere during winter convection as evidenced by elevated CFC-11 concentrations extending across the Labrador Sea above 2200 m as illustrated in AR7W tracer sections for 1997 and 2009 (Figure 2). In contrast, ^{129}I is relatively lower in concentration in these intermediate water masses (Figure 2), because it is supplied to the Labrador Sea mainly by lateral transport from the Nordic Seas. ISOW has the lowest CFC-11 and ^{129}I concentrations (and the highest salinity) reflecting its long ventilation time scales while the fresher, colder underlying DSOW has the highest CFC-11 and ^{129}I tracer levels owing to its direct input pathway via near surface waters in the Nordic Seas [*Smith et al.*, 2005]. ^{129}I concentrations in all Labrador Sea water masses increased markedly between 1997 and 2009 while CFC-11 concentrations increased only modestly during this time. In DSOW ^{129}I increased by about 350% while CFC-11 increased by only about 25%. This reflects the large increase in the ^{129}I input function at Denmark Strait in the late 1990s and early 2000s (Figure 1, inset) and the leveling off of CFC-11 in the atmosphere following the early 1990s due to the Montreal Protocol.

A more complete illustration of the temporal development of hydrographic properties and tracer concentrations in DSOW through 2014 for sampling stations on the AR7W line is illustrated in Figure 3. The bottom axis represents the station distance eastward from the Canadian shelf (Figure 1). The density of the near-bottom core of the DSOW fluctuates significantly in time. Therefore, the core of DSOW in the Labrador Sea is better defined by a range of elevations from the seafloor rather than by ranges of density or other seawater properties. In this study, the ISOW-DSOW boundary was defined by the 28.13 neutral density surface, but operationally DSOW could be viewed as the water layer within a 100 m range off the seafloor in order to average tracer properties [*Yashayaev*, 2007].

Between 1965 and 2005 the DSOW in the Labrador Sea cooled and freshened by about 0.4°C and 0.05, respectively [*Dickson et al.*, 2002; *Yashayaev*, 2007]. In addition to the long-term trends, the near-bottom layer of the DSOW-derived water exhibited large interannual variations in temperature and salinity [*Yashayaev and Dickson*, 2008]. There is a high coherence evident in Figure 3 of the near-bottom changes in T and S across the Labrador Sea caused by the passage of anomalously cold and fresh events spreading from the

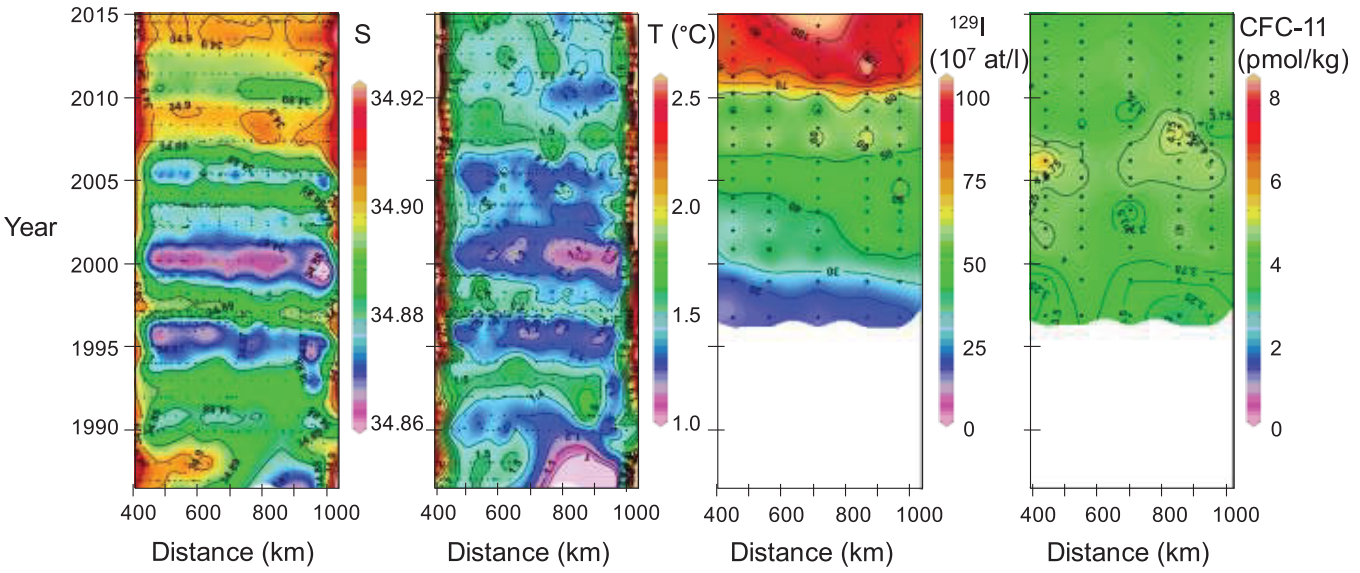

Figure 3. Salinity, temperature, ^{129}I, and CFC-11 time series for DSOW (mean values for bottom 100 m, Figure 2) in Labrador Sea on AR7W line. The S and T time series exhibit interannual variability on a 5 years cycle from freshwater anomalies spreading east to west. The ^{129}I time series exhibits two sharp increases in 2001 and 2011, respectively, spreading westward across the Labrador Sea on a 1 year time scale while the CFC-11 levels remain relatively constant over this time period.

Irminger Sea. At the same time there is a distinct and mostly systematic lag in the arrival of the observed DSOW signals from the Greenland to the Labrador side of the AR7W line. For example, cold, fresh events arriving from the Irminger Sea, in most cases first appear on the eastern side of the Labrador Sea and exit about a year later on the western side. Although both salinity and temperature signals are relatively strong and distinct, the salinity variations tend to have a higher spatial regularity compared to the corresponding temperature variations. In some cases the signals reach the western side of AR7W before the central basin. This is likely due to faster advection of anomalies with the deep boundary current along the margins of the Labrador Sea. The westward spreading of the T and S hydrographic anomalies across the Labrador Sea is characterized by S and T maxima having a periodicity of about 5 years (e.g., maxima in T and S occur in 1992–1993, 1997–1998, 2004, 2008–2009, and 2014).

^{129}I levels in DSOW exhibit two sharp increases in 2001 and 2011, respectively (Figure 3). The first increase represents the arrival of the leading edge of the late 1990s increase in ^{129}I levels in the Nordic Seas (Figure 1). The second ^{129}I increase may represent the delayed arrival of the same late 1990s ^{129}I increase that had separated from the initial pulse in the Nordic Seas and undergone northward transport into the Arctic Ocean with the Fram Strait Branch Water (FSBW) component of Atlantic Water [*Smith et al.*, 2011]. It then followed the Lomonosov Ridge in an "arctic loop" current [*Mauritzen*, 1996; *Smith et al.*, 2011; *Rudels et al.*, 2013] and turned southward in the East Greenland Current to emerge approximately 10 years later in DSOW in the Labrador Sea (Smith and Karcher, unpublished manuscript). Similar to the above noted S and T anomalies, the ^{129}I concentration increase between 1997 and 2001 appears to track westward across the Labrador Sea with a time lag between its appearance in eastern and western regions of about 1 year (Figure 3).

3.4. Line W Results

Line W represents an observational system designed to quantify the properties, structure, and transport of the waters of the Northwest Atlantic DWBC [*Toole et al.*, 2011; *Pēna-Molino et al.*, 2011]. It consists of a moored array spanning the US continental slope and a program of repeated ship-based hydrographic/direct-velocity sections along the array extending southeast toward Bermuda (Figure 1). Locally, the bathymetry is steep and cross-structurally uniform along the continental slope, topographic characteristics that appear to focus and stabilize the DWBC over a narrow depth and lateral range. The subthermocline water column corresponding to the DWBC on Line W is composed of water masses (Figure 1) whose neutral density limits (γ^n) were defined by *Pickart and Smethie* [1998] and revised by *LeBel et al.* [2008] for the various classes of LSW (27.83–27.98), ISOW (27.98–28.066), and DSOW (>28.066). Technically, the boundary between ISOW and underlying DSOW may be best defined as the maximum vertical salinity gradient

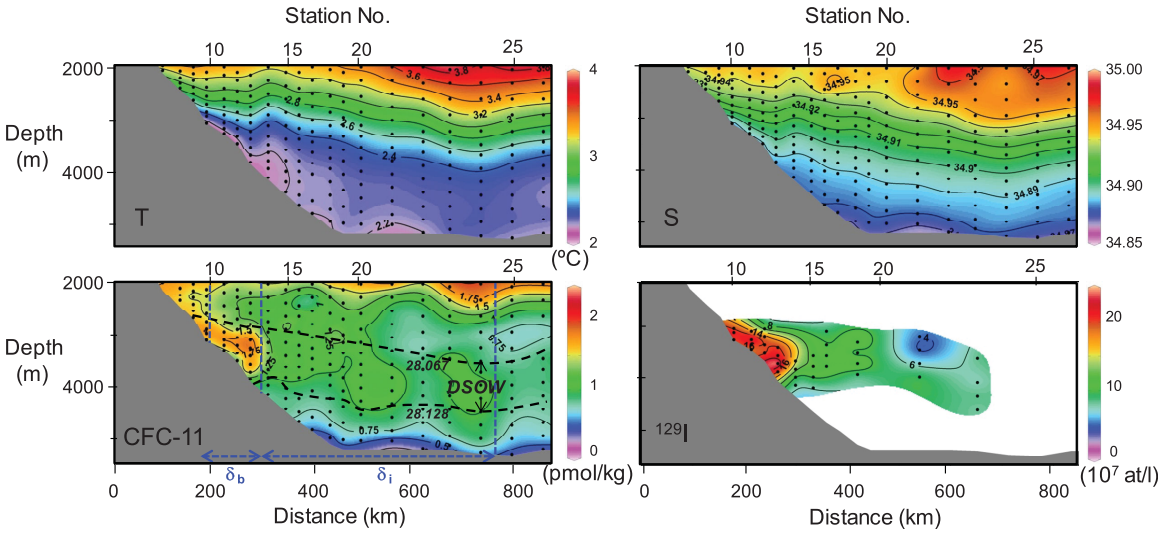

Figure 4. Sections for S, T, CFC-11, and ^{129}I on Line W measured in 2012. Dashed line contours in CFC-11 section illustrate neutral density (γ^n) boundaries for DSOW. The core of the DWBC is positioned adjacent to the slope at a depth of about 3500 m and is delineated by local minima in T and S and local maxima in tracers CFC-11 and ^{129}I. Based on the CFC-11 section, the core width (δ_b) is 100 km (delineated by vertical blue dashed lines) and the interior (shoulder) width (δ_i) is 460 km to give a model value for α ($=\delta_b/\delta_i$) of 0.22 in 2012.

between these two water masses [*Lebel et al.*, 2008]. In the interior, the core DSOW lies above the colder, fresher northward flowing AABW. *LeBel et al.* [2008] chose the $\gamma^n = 28.158$ surface to mark the transition between the two in the western North Atlantic. However, for the purposes of the present study core DSOW is best described by maxima and minima in tracer concentrations.

DSOW appears as a core of high CFC-11, ^{129}I, and oxygen and a local lateral minimum in salinity and temperature banked against the continental slope at depths of 3000–4000 m (Figure 4). It is distinguished by a pattern of sloping isopycnals tilted deeper offshore that are indicative of increased equator flow of water compared to the overlying ISOW. Time series suites of CFC-11 and ^{129}I tracer sections undertaken on Line W between 2004 and 2013 are illustrated in Figures 5 and 6. Although the ^{129}I sampling distribution was sparser than that for CFCs, the core of the DWBC is readily discernible in the ^{129}I sections. The resolution of the ^{129}I core is enhanced compared to that of the CFC-11 core (Figure 4), because ^{129}I levels are comparatively lower in the overlying water masses, ISOW and LSW [*Smith et al.*, 2005] and ^{129}I is virtually absent from AABW. The configuration of the DWBC core was delineated by CFC-11 tracer values within 20% of the maximum values measured on each section below 3000 m. This generally comprised 5–10 samples that spanned three stations over a distance of 70–100 km and included samples from several water depths (separated by 150–200 m) at each station. ^{129}I values for core DWBC water were determined from the detailed core configuration outlined by the CFC-11 data. The width of the core determined in this manner usually ranged from 20 to 30% of the width of the interior shoulder region which stretches between the core and an abyssal region of sharply diminished tracer concentration gradients. The penetration of tracers and other water properties from the DWBC to the interior shoulder region is governed by mixing and exchange processes for the two regions. In the Newfoundland Basin, the tail of the Grand Banks causes some of the DWBC water to be recirculated into the interior [*Bower et al.*, 2009]. Near Cape Hatteras southwest of Line W, the DWBC crosses beneath the Gulf Stream, and some DWBC water recirculates into the interior and forms the Northern Recirculation Gyre, which extends 100–300 km seaward from the DWBC between 65°W and the tail of the Grand Banks [*Hogg et al.*, 1986; *Pickart and Smethie*, 1993; *Bower and Hunt*, 2000a,2000b]. Exchange with the shoulder region is also enhanced by deep cyclones that form beneath the troughs of Gulf Stream meanders between Cape Hatteras and the tail of the Grand Banks [*Andres et al.*, 2016].

3.5. Bermuda Rise Results

The 2010 transect over the Bermuda Rise (Dynamite Line; Figure 7, inset) extending Line W southeastward past Bermuda was designed to intercept the southwestward flow of DSOW across the Atlantic abyssal plain. The ^{129}I and CFC-11 sections on the southern Bermuda Rise are illustrated in Figure 7. A core of recently .ventilated water having elevated concentrations of ^{129}I and CFC-11 (and low T and S, not shown) is evident at

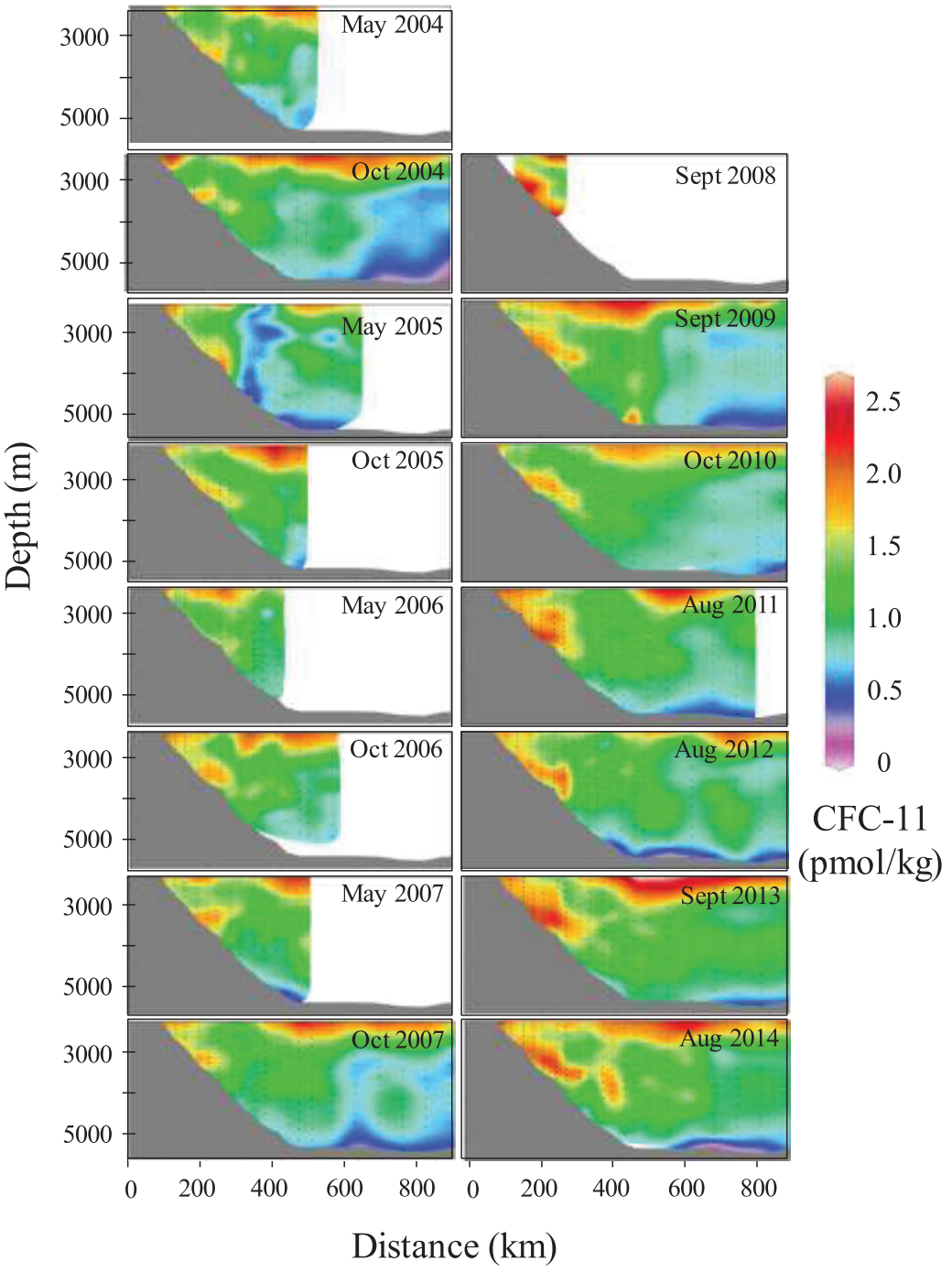

Figure 5. CFC-11 sections for Line W (2004–2014). The DSOW core of the DWBC outlined by elevated CFC-11 concentrations at depths of 3000–4000 m adjacent to the continental slope is usually 70–100 km wide. CFC-11 levels in the interior shoulder region are governed by core-interior mixing and recirculation, processes parameterized in the model using t_{mix}.

a depth of 3500 m at the base of the southern Bermuda continental slope. ^{129}I levels in the tracer core over the Bermuda Rise are in the 5–10 at/l $\times$ 10^7 range compared to levels of 10–20 at/l $\times$ 10^7 measured in the core of the DWBC in 2010. Similarly, CFC-11 levels measured in the high tracer core water over the Bermuda Rise of 0.8 pmol/kg are lower by a factor of about 2 compared to those measured in 2010 on Line W. The analysis of Bermuda Rise hydrographic results indicates that the core water is a mixture of DSOW and AABW that has undergone significant modification during separation from the DWBC and transport through the interior.

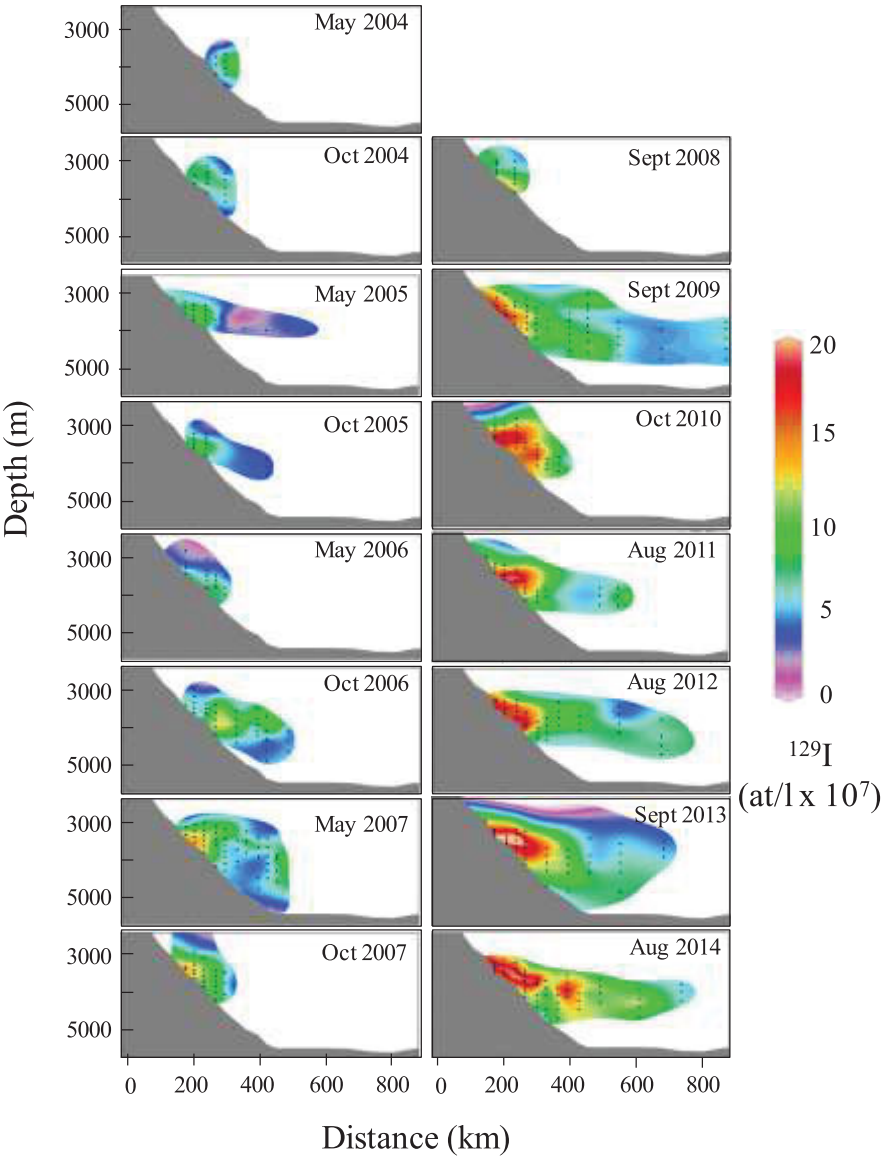

Figure 6. ^{129}I sections for Line W (2004–2014). The DSOW core of the DWBC is outlined by elevated ^{129}I concentrations at depths of 3000–4000 m adjacent to the continental slope following the more detailed pattern defined by the CFC-11 sections (Figure 5). Core ^{129}I concentrations increased by 300% (from 8 to 23 at/L $\times$ 10^7) between 2004 and 2014 following the large ^{129}I time series increases in DSOW upstream in the Labrador Sea (Figures 2 and 3).

4. Discussion

4.1. Boundary Model Applications

The Labrador Sea and Line W tracer time series studies provide a basis for directly tracking the flow of DSOW between the Labrador Sea and deep North Atlantic without having to rely on generic estimates of tracer inputs to the ocean. In Figure 8 (bottom) the time series for vertical profiles of ^{129}I through DSOW (defined by dashed line in Figure 8) in the Labrador Sea is illustrated for Sta. 17 which is the deepest and most centrally located Labrador Sea station on Line AR7W (Figure 2). Figure 8 (top) shows the time series of vertical profiles of ^{129}I in the boundary current on Line W, measured from the bottom through the DSOW core for each year of the 2004–2014 time series sections from Figure 6. This time series shows that the high ^{129}I core of DSOW (delineated by dashed lines in Figure 8) in the boundary current is usually located about 200–300 m off the bottom. An approximate doubling of the ^{129}I concentration in DSOW was first observed on the AR7W section in 1999–2001 and subsequently observed in

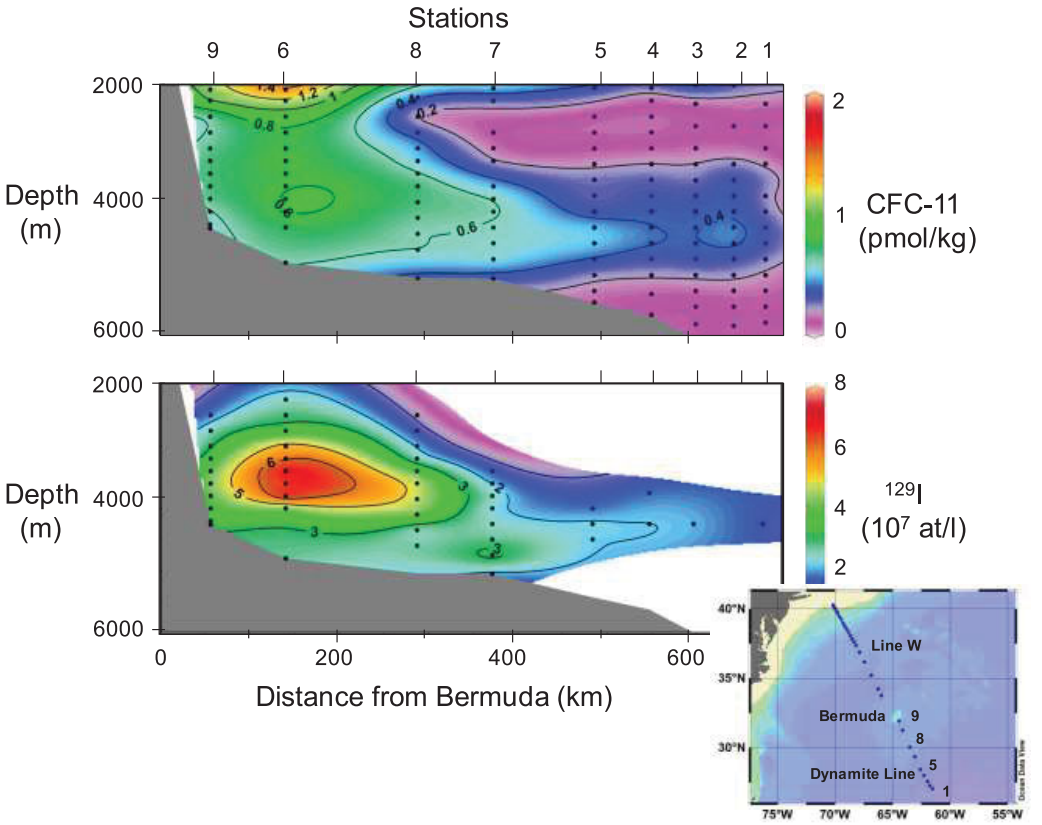

Figure 7. (top) CFC-11 section on Dynamite Line extending south-eastward from Bermuda over Bermuda Rise. (bottom) ^{129}I section on Dynamite Line. Inset shows positions of Dynamite Line stations and Line W relative to Bermuda. The core of DSOW that has separated from the DWBC and been transported through interior pathways over Bermuda Rise is delineated by tracer maxima adjacent to southern Bermuda slope.

core DSOW on Line W in 2006–2007 (Figures 8 and 9) implying a transit time between the two locations of 5–8 years.

The time series data sets for the mean concentrations of CFC-11 and ^{129}I for DSOW on the AR7W line and in core and interior DSOW on Line W are summarized in Figure 9. For this figure, the Labrador Sea tracer concentrations were calculated giving equal weight to each of the five standard sampling stations for ^{129}I (Figure 2) on the AR7W line, with the exception of the 1993 data [*Smith et al*., 2005] which are from *Edmonds et al*. [2001]. The tracer levels for DSOW in the boundary current core for each Line W section were calculated as the mean value for the suite of measurements within 20% of the maximum level. This constraint also determined the position of the outer edge of the boundary current core. The CFC-11 tracer value for the interior region was then calculated as the mean value for the suite of measurements extending from the outer edge of the core to the point at which tracer levels had decreased below the core value by a factor of 2. The value of α (ratio of the widths of the core and interior regions) determined in this manner had a mean value of about 0.25. The method for calculating α is illustrated graphically in the CFC-11 section of Figure 4 by the blue dashed lines outlining the dimensions of the boundary core (width δ_b) and interior (width δ_i) regions. In most cases, the ^{129}I data set was insufficient to permit an accurate determination of ^{129}I levels through the complete interior region. In these cases, the ^{129}I levels in the interior region were assumed to be equal to the product of the mean ^{129}I/CFC-11 ratio for the available interior data and the remaining interior CFC-11 data. In some cases the CFC-11 sections did not extend to the edge of the interior region as defined above. In these cases, an algorithm was calculated for tracer gradients in sections for which the core-interior levels were well defined (e.g., October 2004 and 2009) and fitted to the available core and interior tracer distributions for incomplete sections to derive the interior tracer values.

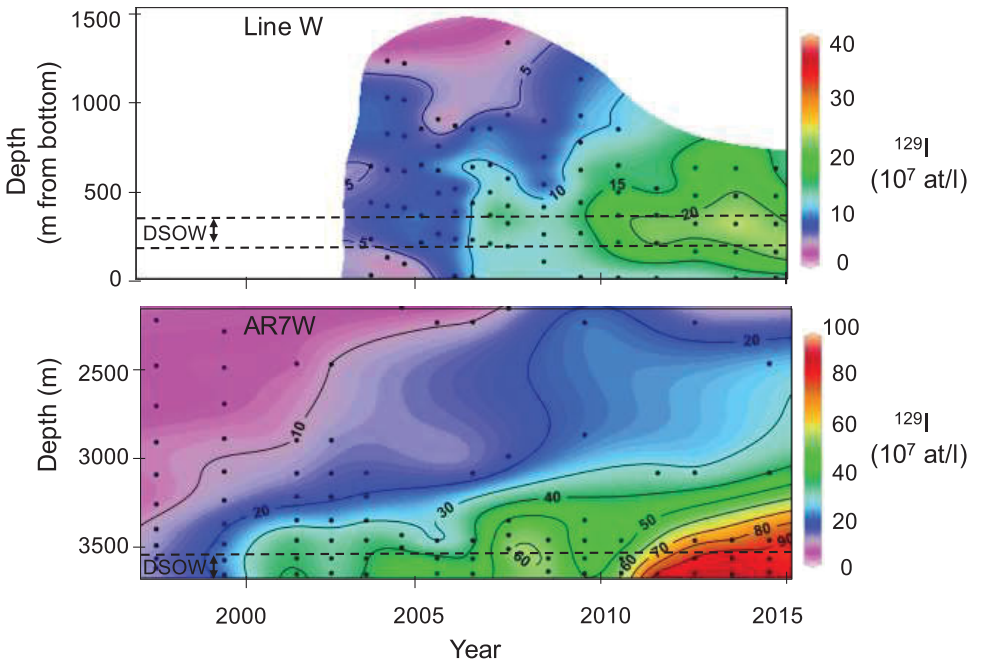

Figure 8. (top) Time series for ^{129}I levels versus depth measured upward from the bottom through core DSOW (delineated by dashed lines) on Line W. Lateral position of the core varies between stations 11 and 13 for a given year. (bottom) Time series for ^{129}I in DSOW (dashed line) at centrally located Sta. 17 on AR7W section. The large ^{129}I increase in DSOW at Sta. 17 on AR7W section in 1999–2001 arrives at Line W in about 2007 implying a transit time between the two locations of 5–8 years.

4.2. Input Functions

In order to constrain advection and mixing rates on Line W using a boundary current model, tracer input functions are required as a time series for DSOW in the Labrador Sea extending to the time of introduction of these tracers into the ocean. The CFC-11 input function was constructed by calculating the ratios of the tracer concentrations in the DSOW input function [*LeBel et al.*, 2008] (Figure 1, inset; lagged by 2 years to account for transport from ventilation regions to the Labrador Sea) to the AR7W Line CFC-11 results for each year of observation. The average of these ratios was multiplied by the DSOW input values prior to the early 1990s to generate the CFC-11 time history for DSOW on the AR7W line to 1950 (Figure 10, top inset). ^{129}I concentrations in DSOW in the Labrador Sea can be approximated by exponential growth ($\sim\exp(t/T_{\exp})$) during the 1993–2014 period with a value of $T_{\exp} = 9.8$ years; ($r^2 = 0.92$) as illustrated in Figure 9 (middle). The entire ^{129}I input function was then constructed by adding the extrapolated, pre-1993 component of this growth concentration curve to the measured AR7W Line ^{129}I time series (Figure 10, bottom inset). These tracer time series for DSOW in the Labrador Sea are then used as input functions, $\chi(0, t-t')$ in equation (3) to calculate tracer values on Line W for given TTDs. The TTDs, $G_b(x,t)$, and $G_i(x,t)$ in equations (4) and (5) for the boundary current core and interior, respectively, are defined by the three parameters, α, t_{adv}, and t_{mix}. Given values of these parameters can then be used in equation (3) to determine model simulations for tracer time series values which are then compared to the experimental results.

4.3. Dependence on t_{adv} and t_{mix}

The boundary current model was run for a range of values for t_{adv}, t_{mix}, and α for core and interior regions. The value of $\alpha = 0.25$ was determined empirically as described above from the CFC-11 time series sections. Model simulations of tracer time series for $t_{adv} = 6$ years and $t_{mix} = 3$ years provide results in agreement with measured tracer distributions for CFC-11 (Figure 10, top) and ^{129}I (Figure 10, bottom) for both core and interior regions of Line W. Comparisons of simulations for $t_{adv} = 6$ years and $t_{mix} = 1$, 3, and 6 years are illustrated in Figure 11 for core (left figures) and interior (right figures) tracer levels on Line W. Since t_{mix} is a relaxation time for tracer exchange between the boundary current core and the interior regions, increasing the value of t_{mix} represents a decrease in the rate of mixing. Increasing the value of t_{mix} from 1 to 6 years for constant t_{adv} (Figure 11, left) results in higher tracer levels in the core of the boundary current, because a smaller proportion of the core tracer signal has been mixed into the interior region of the boundary current

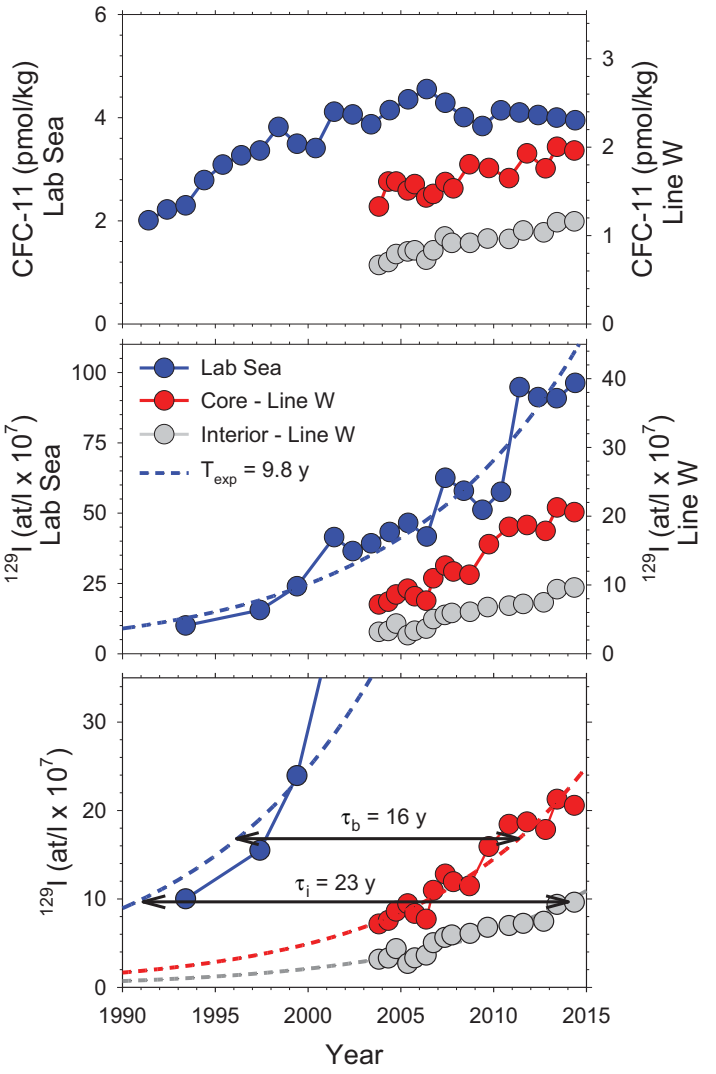

Figure 9. (top) CFC-11 time series concentrations for DSOW in Labrador Sea (blue symbols) on left hand axis, and for CFC-11 in DSOW boundary current core (red symbols) and interior (gray symbols) on Line W (right-hand axis). (middle) ^{129}I concentrations for DSOW in Labrador Sea (left-hand axis) and for DSOW in boundary current core and interior on Line W (right-hand axis). Dashed lines represents exponential fits to ^{129}I time series for DSOW in Labrador Sea (r^2 = 0.92, with time constant, T_{exp} of 9.8 years); DWBC core (r^2 = 0.92 with T_{exp} = 9.3 years); DWBC interior (r^2 = 0.86 with T_{exp} = 8.9 years). (bottom) Comparison of exponential fits to ^{129}I time series for DSOW in Labrador Sea with Line W (shown by black arrows) gives tracer ages, τ, of 16 and 23 years for boundary current core and interior ^{129}I time series, respectively.

by the time of its arrival at Line W. Tracer levels in the interior region exhibit a more complex dependence on t_{mix} (Figure 11, right). For a value of t_{adv} = 6 years, interior tracer levels pass through a maximum with t_{mix} increasing from a value of 1–6 years and eventually decline to zero as mixing rates approach zero and boundary current flow becomes completely advective.

The level of agreement of the model results with the Line W tracer data for a given range of parameter values for α, t_{adv}, and t_{mix} can be evaluated from the root mean squares (RMS) of the sums of the errors between model and experimental results [*Mauldin et al*., 2010]. The model was run for values of the parameters, t_{adv} and t_{mix} in the range of 0–15 years with the RMS errors for each set of parameter values weighted equally for each separate occupation of Line W. The RMS errors for ^{129}I are illustrated in Figure 12 for the core and interior regions (top two figures) as a function of parameter values, t_{adv} and t_{mix} (α = 0.25). A trough representing minimum values of the RMS errors for core ^{129}I increases monotonically with increasing t_{mix} over a range of t_{adv} = 3–10 years (Figure 12, top). In contrast, a trough for minimum RMS for interior ^{129}I passes through a maximum value of t_{adv} (near t_{mix} = 3 years) before decreasing monotonically with increasing t_{mix} (Figure 12, middle). Combining the two RMS distributions weighing each equally results in a distribution (Figure 12, bottom) for which an absolute minimum occurs in the range of t_{adv} = 5–6 years, t_{mix} = 2–4 years. RMS distributions for core and interior CFC-11 are illustrated in Figure 13. These are similar to those of ^{129}I, but the minima are less well defined. The combined distributions for CFC-11 (Figure 13, bottom) also give an absolute minimum in the same range of t_{adv} = 5–6 years, t_{mix} = 2–4 years as evident in the ^{129}I analysis, but with shallower contour gradients. The range in advection times (5–6 years) corresponds to a range of flow velocities at the Line W location, 4600 km downstream of the Labrador Sea, of u = 2.4–2.9 cm/s.

Mauldin et al. [2010] applied the same boundary current model used in the present study to the tracer combination of ^{3}H and ^{3}He:^{4}He in the flow of Barents Sea Branch Water (BSBW) along the marginal slope of the Arctic Ocean through the Eurasian, Makarov, and Canada Basins. They used a value for α of 0.2 based on measurements of CFC-11 sections across the Eurasian Basin for which the actual width of the core of the boundary

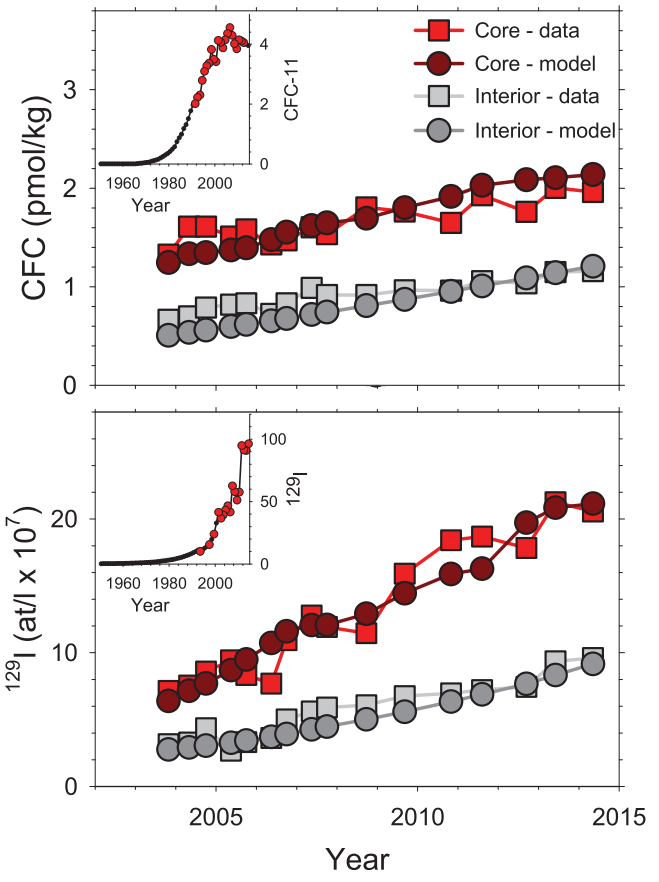

Figure 10. Boundary current model simulations using the parameter values, $t_{adv} = 6$ years; $t_{mix} = 3$ years; $\alpha = 0.25$ are compared to experimental tracer results for core and interior regions for CFC-11(top) and ^{129}I (bottom). Model input functions are given in insets for CFC-11 (pmol/kg; top) and ^{129}I (at/L $\times$ 10^7; bottom) for DSOW in Labrador Sea with actual data points given by red symbols.

current was about 35 km, or close to half the width of the DWBC core. Their comparisons of model simulations to tracer measurements along the boundary current axis of flow resulted in parameter estimates of $u = 2.5$ cm/s and $t_{mix} = 6.5$ years. These results indicate that the advection velocities are similar for the deep boundary currents of the Arctic and North Atlantic Oceans. The more rapid mixing ($t_{mix} = 2.6$ years) determined for the DWBC may reflect enhanced core-interior exchange resulting from the recirculation processes described above.

4.4. Analytical Model Solution

Analytical solutions for model parameters can be determined for the special case of tracer input functions that exhibit exponential growth; i.e., $\chi(0,t) = \exp(t/T_{exp})$. As noted above, ^{129}I levels in DSOW in the Labrador Sea can be approximated by exponential growth through the 2000s with a value of $T_{exp} = 9.8$ years (Figure 9). Exponential growth equations can also be fitted to the ^{129}I time series for the core ($T_{exp} = 9.3$ years; $r^2 = 0.92$) and interior ($T_{exp} = 8.9$ years; $r^2 = 0.86$) regions (Figure 9). CFC-11 growth in the Nordic Sea overflow waters was approximately exponential through the 1980s [*Pickart et al.*, 1989], but has slowed since then with CFC-11 concentrations in DSOW beginning to decline in the 2000s (Figure 9).

In the present study, the tracer ages, τ_b and τ_i, represent the time lags between observation times of DSOW tracer concentrations in the boundary current core and interior waters, respectively, on Line W and times of upstream DSOW tracer signal measurements having the same concentrations on the AR7W line in the Labrador Sea. This differs from the usual definition of tracer age as the time elapsed since the water mass left the mixed layer [*Rhein et al.*, 2015], because tracer age in this study is referenced to tracer levels in DSOW in the Labrador Sea rather than to levels in surface water in contact with the atmosphere. The determination of the tracer ages, τ_b and τ_i for ^{129}I of 16 and 23 years, respectively, is illustrated by black arrows in Figure 9 where the tracer ages are referenced to the exponential fit to the ^{129}I time series for the Labrador Sea. Note that the core tracer age of 16 years exceeds the range (5–6 years) estimated above for the core advection time. The reason is that for purely advective flow the tracer age represents the time elapsed since the downstream volume element of water was last present at the upstream location, but mixing acts to increase the tracer age to an extent in accordance with the configuration of the tracer input function. The distance between the AR7W Line and Line W (4600 km) divided by the ^{129}I tracer age represents the tracer spreading rate, υ which is 0.9 cm/s for core boundary current water. The boundary current flow velocity is the quantity that should most closely simulate in situ flow measurements, but the tracer spreading rate governs the transport rates of anthropogenic substances such as atmospheric CO_2 into the ocean interior and the deep water arrival times of upper ocean hydrographic fluctuations driven by high latitude climate variability.

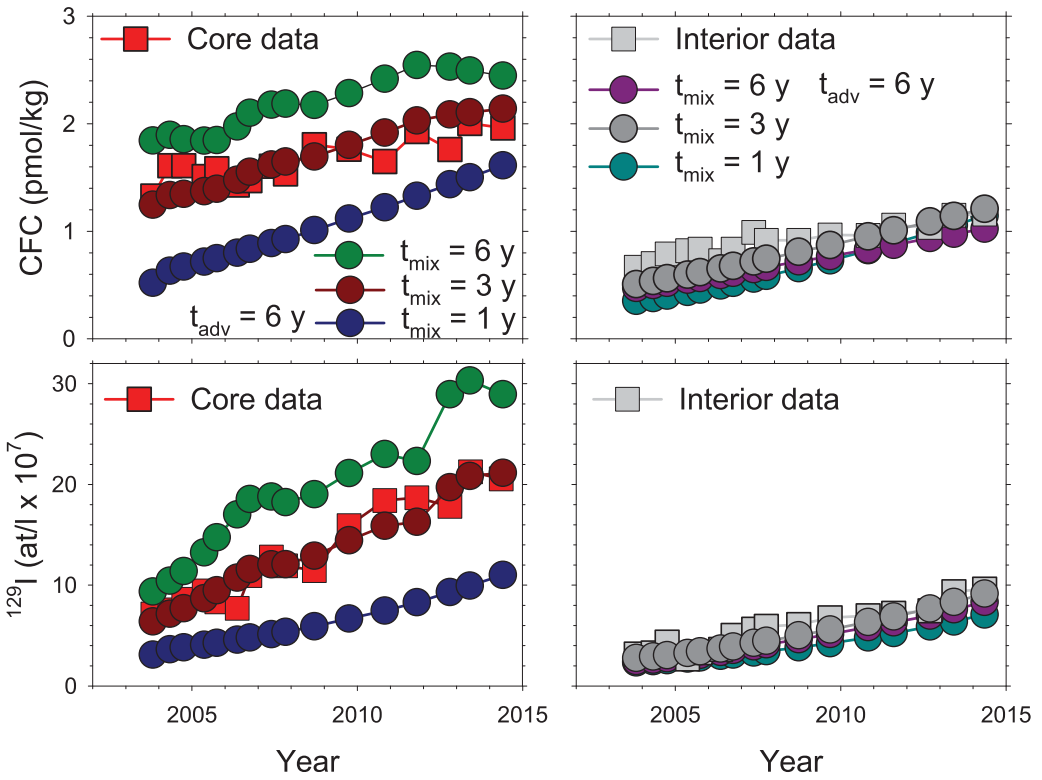

Figure 11. Red square symbols are time series data for CFC-11 (top left) and ^{129}I (bottom left) in core DSOW on Line W. Gray square symbols are time series data for CFC-11 (top right) and ^{129}I (bottom right) in interior water on Line W. Other symbols represent model simulations for $t_{adv} = 6$ years, $\alpha = 0.25$ and different values of t_{mix} as given in the legends. Core tracer levels increase with increasing t_{mix} (decreasing mixing) while interior tracer levels exhibit maxima close to $t_{mix} = 3$ years.

Waugh and Hall [2005] solved equations (1) and (2) for tracers having an exponentially increasing input function and reported the following analytical solutions for tracer ages for core and interior waters, τ_b and τ_i, respectively,

$$\tau_b = t_{adv}\left(1+\frac{1}{(\alpha+t_{mix}/T_{\exp})}\right), \tag{8}$$

$$\tau_i = \tau_b + T_{\exp}\ln\left(1+\frac{t_{mix}/T_{\exp}}{\alpha}\right). \tag{9}$$

In the limit of very large mixing rates ($t_{mix} \ll 1$), $\tau_i = \tau_b$ and tracer concentrations in the interior become equal to those in the core. The tracer ages of the core and interior together approach the value of a parameter referred to as the mean transit time, or mean age, Γ where $\Gamma = t_{adv}(1 + (1/\alpha))$. The mean age Γ is independent of t_{mix} for reasons outlined in detail in *Waugh and Hall* [2005]. As the mixing rate is reduced from very large values (t_{mix} increases) then τ_b decreases (equation (8)) and the core tracer concentration increases monotonically with increasing t_{mix}. This is evident in Figure 11 (bottom left) where core ^{129}I concentrations increase as t_{mix} increases from values of 1–6 years. In the limit of infinitely large t_{mix}, τ_b approaches the value of t_{adv}, flow becomes purely advective and the entire tracer signal is confined to the core of the boundary current. CFC distributions (Figure 11) exhibit a similar dependence on model parameters to ^{129}I, because the CFC input function has been close to an exponentially increasing signal for much of the relevant flow history on Line W.

Interior tracer levels respond quite differently to changes in t_{mix}. At very low values of t_{mix} (rapid mixing regime) and t_{adv}, a decrease in the mixing rate (increase in t_{mix}) produces an increase in τ_i and a monotonic decrease in interior tracer levels. However, for larger values of t_{adv}, an increase in t_{mix} initially produces a

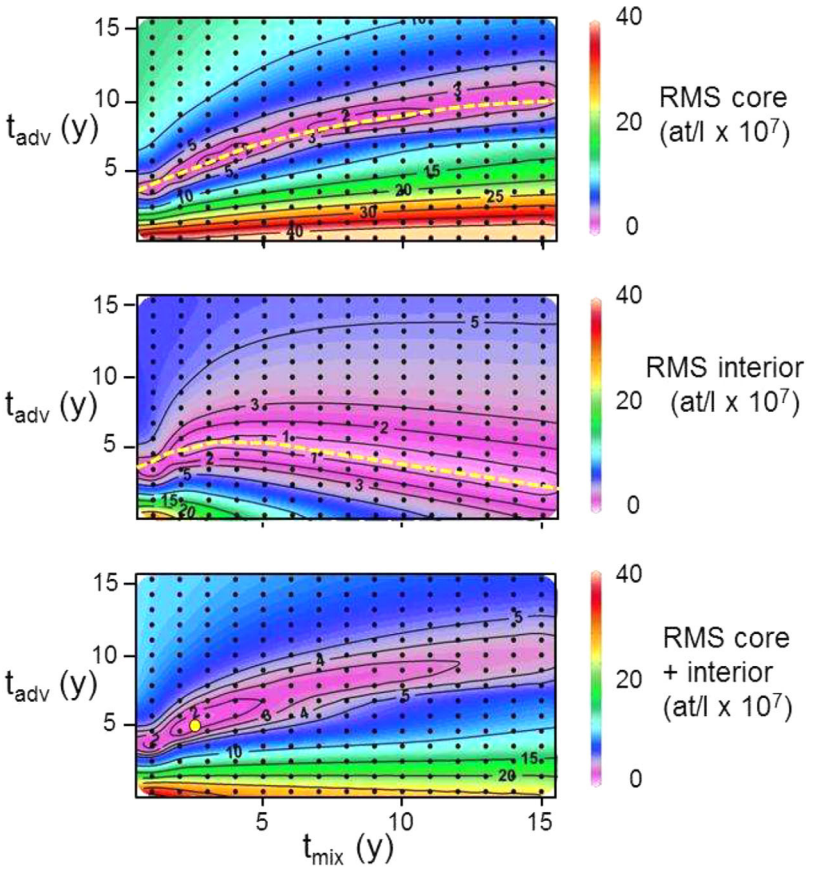

Figure 12. Contoured plots of RMS for t_{adv} versus $t_{mix.}$ (top) Core ^{129}I RMS error. (middle) Interior ^{129}I RMS error: Yellow dashed curves represent analytical solution for exponentially increasing tracer input having T_{exp} = 9.8 years and measured values of τ_b = 16 years; τ_i = 23 years; as outlined in text. (bottom) Combined ^{129}I RMS for core and interior gives crossover minimum in agreement with parameter values of t_{adv} = 5.4 years; t_{mix} = 2.6 years (marked by yellow circle) for analytical solution.

decrease in τ_i and increasing interior tracer levels. As t_{mix} continues to increase then the value of τ_i passes through an inflection point and interior tracer levels attain a maximum value. Interior tracer levels then decline with further increases in t_{mix}, eventually approaching zero as mixing rates approach zero and flow becomes advective. This dependence of interior tracer levels on t_{mix} is evident in Figure 11 (bottom right) where interior ^{129}I levels for values of t_{mix} = 1, 3, and 6 years are highest at t_{mix} = 3 years. The idea that tracer levels in both core and interior components of the boundary current can increase simultaneously with decreasing mixing rates in downstream (larger values of t_{adv}) regimes may seem counter-intuitive. However, the additional supply of tracer required to meet this condition occurs from the depletion of upstream (lower t_{adv}) interior regimes. It is this contrast in their dependence on t_{mix} between the core and interior tracer levels that permits the determination of the model parameters, t_{adv} and t_{mix} from individual tracer sections.

The relationship between t_{adv} and t_{mix} for ^{129}I in the core of the boundary current for the measured parameter values (τ_b = 16 years; T_{exp} = 9.8 years; α = 0.25) is defined by equation (8) and is illustrated by the dashed line in the upper panel of Figure 12. The relationship between t_{adv} and t_{mix} for ^{129}I in the interior for τ_i = 23 years as defined by the combined equations (8) and (9) is illustrated by the dashed line in Figure 12 (middle). The good agreement of the dashed curves with the minima in the RMS contoured plots (Figure 12) is consistent with an exponentially increasing ^{129}I input function. The simultaneous solution of equations (8) and (9) gives values of t_{adv} = 5.4 years, t_{mix} = 2.6 years illustrated by a yellow symbol in Figure 12 (bottom) that are within the parameter ranges of t_{adv} = 5–6 years, t_{mix} = 2–4 years determined in the previous section by minimizing the RMS error. The value of t_{adv} = 5.4 years corresponds to a core boundary current flow velocity, u of 2.7 cm/s.

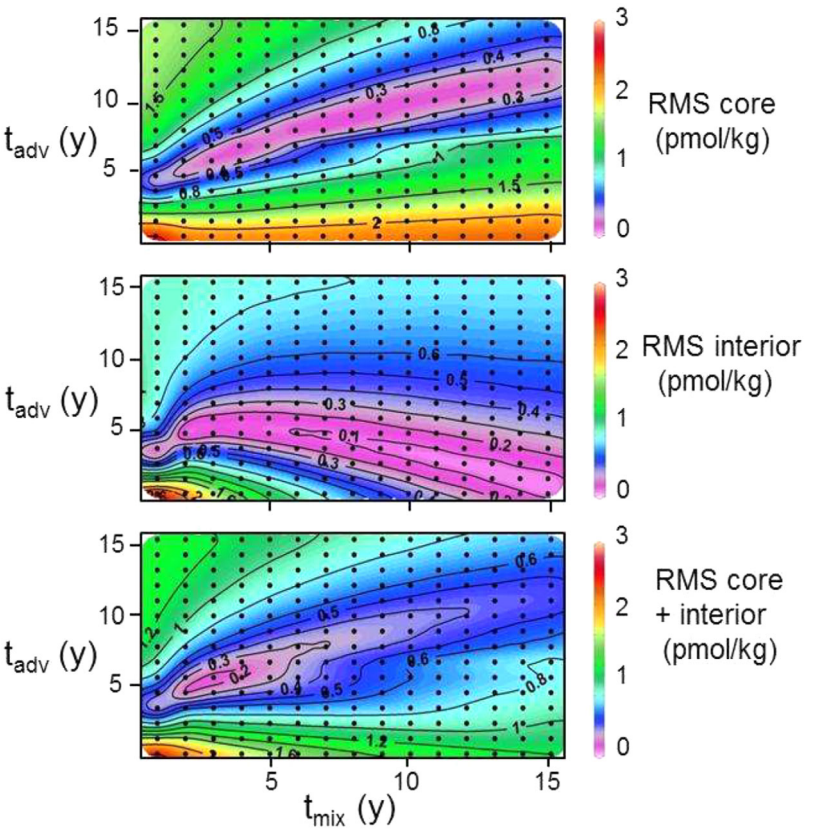

Figure 13. Contoured plots of RMS for t_{adv} versus t_{mix} for CFC-11 and $\alpha = 0.25$. (top) Core CFC-11 RMS error; (middle) interior CFC-11 RMS error; (bottom) combined CFC-11 RMS error for core and interior gives minimum for parameter values in the range; t_{adv} = 5–6 years; t_{mix} = 2–4 years.

4.5. Determination of α

Applications of the boundary current model to tracer flow rely on an empirical determination of the value of α. The relationship between α, t_{mix}, and t_{adv} for the Line W ^{129}I time series results; $T_{exp} = 9.8$ years, $\tau_b = 16$ years; $\tau_i = 23$ years is defined by equations (8) and (9) and is illustrated by the solid line in three-dimensional t_{mix}, t_{adv}, and α coordinate space in Figure 14. Increasing the value of α broadens the core of the boundary current relative to the interior and as a result equations (8) and (9) require slower flow (greater advection time, t_{adv}) and reduced mixing rates (greater t_{mix}) in order to conform to the measured ^{129}I tracer ages for core and interior flow. Projections of the curve in Figure 14 onto the $t_{adv} - t_{mix}$ plane are illustrated by the red dotted curves. The yellow drop line is for the value of α (=0.25) that conforms to the present study and corresponds to $t_{adv} = 5.4$ years; $t_{mix} = 2.6$ years as given by equations (8) and (9).

Waugh and Hall [2005] developed the present boundary current model and applied it to a data set of ventilation tracers (tritium, tritium-helium, CFC-11, and CFC-12) measured in the core of the DWBC. They employed a value for α of 0.1 and reported good agreement between model and measured results for values of $u = 5$ cm/s (corresponding to a value of about $t_{adv} = 3$ years at Line W) and $t_{mix} = 1$ year. *Doney and Jenkins* [1994] employed a similar type of "leaky pipe" model in a study of tritium-helium flow in the DWBC and simulated their data sets using $u = 5$ cm, t_{mix} = 1–2 years, and α = 0.03–0.13. These studies relied on tracer measurements at different locations along the flow axis of the DWBC and did not require agreement between model and interior tracer concentrations which were not always measured. In contrast, the present study relies on a time series of tracer sections across the flow axis of the DWBC at Line W for which both the core and interior tracer concentrations are used to constrain model simulations. If a value of $\alpha = 0.1$ is used in equations (8) and (9) together with the measured parameter values of T_{exp}, τ_b, and τ_i for ^{129}I in the DWBC, then the result is $t_{adv} = 2.7$ years ($u = 5.4$ cm/s at Line W) and $t_{mix} = 1.0$ year. Accordingly, the

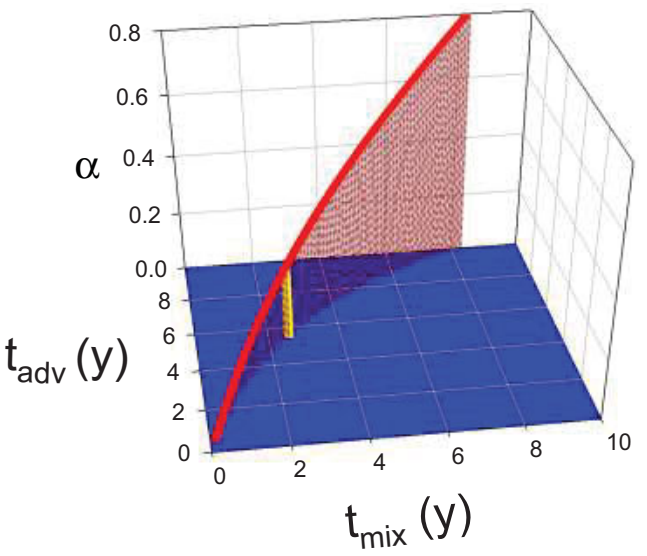

Figure 14. The solid red curve represents the model relationship between α, t_{mix}, and t_{adv} for an exponentially increasing tracer input where $T_{exp} = 9.8$ years, $\tau_b = 16$ years; $\tau_i = 23$ years. Yellow drop line is for the experimentally determined value of $\alpha = 0.25$ and intersects the t_{adv}-t_{mix} plane at $t_{adv} = 5.4$ years; $t_{mix} = 2.6$ years.

present tracer study would provide good agreement between model simulations and core and interior tracer results for values of t_{adv} and t_{mix} close to those of previous studies if the value of $\alpha = 0.1$ rather than $\alpha = 0.25$ had been employed.

The value of $\alpha = 0.25$ is a mean value estimated from the configurations of CFC-11 tracer sections that are sufficiently well defined within the interior region to provide good evaluations of alpha. There is considerable annual and bi-annual variability in this value of α for which the range is about 0.1–0.4 based on this 10 years study. This temporal variability in α is notably influenced by the effects of highly variable Gulf Stream meanders on deep circulation which can significantly influence rates of exchange between core and interior waters [*Andres et al.*, 2016].

4.6. Bermuda Rise Signal

The Bermuda Rise section provides only a single temporal view of the tracer distributions, but it is useful to consider these data in the context of the boundary current model. The flow of DSOW above the steep eastern flank of the Bermuda Rise with high concentration tracer cores appears to be remarkably coherent and steered equatorward by the topography. Accordingly, the boundary current model was applied to obtain a first approximation of advection times and mixing rates. It is not possible to accurately constrain the dimensions of the DSOW core from the sparse data set, so it is assumed that its configuration is similar to that of DSOW on Line W and can be characterized by a value of $\alpha = 0.25$. The mean values of ^{129}I levels in the core and interior of the Bermuda Rise section (Figure 7) are estimated to be equal to 6×10^7 at/L and 2.5×10^7 at/L, respectively, from the measured distribution along the section. These values can be compared to the ^{129}I Labrador Sea input function (Figure 10) to give values for the tracer ages of $\tau_b = 24$ years and $\tau_i = 33$ years. Equations (8) and (9) then give values of $t_{adv} = 9$ years and $t_{mix} = 4$ years for the boundary current flow through the interior. The longer advection time of 9 years for flow over the abyssal plain to the Bermuda Rise compared to 5.4 years in the DWBC to Line W would seem reasonable as the interior flow would be expected to be comparatively more sluggish and/or meandering. *Curry et al.* [1998] estimated a time lag of about 6 years for the transport of LSW to Bermuda based on comparisons of hydrographic time series measurements for both intermediate water regimes, but lag times need not be the same for LSW and underlying DSOW. Since the specific flow pathway is not known for flow through the interior it is not possible to estimate a flow velocity for the model advection time of 9 years for the Bermuda Rise. The mixing time constant of $t_{mix} = 4$ years indicates slightly less rapid, core-shoulder mixing within the interior current regime compared to that for Line W.

4.7. Propagation of Hydrographic Anomalies

The propagation of temporal variations in temperature and salinity between the Labrador Sea and Line W can be evaluated by applying the boundary current model to the simulation of idealized tracers with periodic boundary conditions. *Waugh and Hall* [2005] showed that when the period, $T_\omega/2\pi$ of the tracer variation is much shorter than the mixing time, t_{mix} then the propagation time of the phase of the signal or phase lag, τ_ω, approaches the value of t_{adv} and the amplitude, A_ω of the tracer variation approaches a value of exp ($-t_{adv}/t_{mix}$). Under these conditions, the tail of the TTD extends over several tracer cycles which thereby cancel and, as a result the mixing component of the TTD contributes negligibly to the overall advective velocity. The amplitude of the signal is then equal to the magnitude of the advective spike.

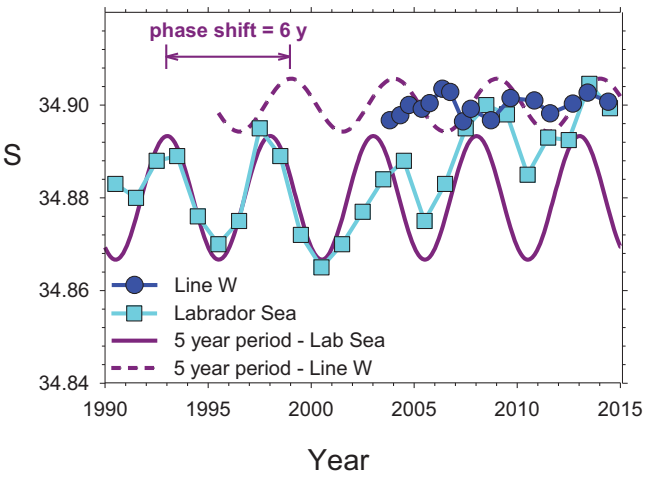

Figure 15. Cyan and blue symbols are salinity plotted as function of time for DSOW on Line AR7W in the Labrador Sea and Line W, respectively. Labrador Sea signal is approximated by sine wave having a period of 5 years (solid dark pink curve). This periodic signal is used as the input function for boundary current model with $\alpha = 0.25$ and a positive offset from Labrador Sea salinity by a constant value of 0.02. A model result for parameters; $t_{adv} = 6$ years; $t_{mix} = 3$ years illustrated by upper dashed curve is compared to Line W data.

The time series for salinity distributions for DSOW along the AR7W line in the Labrador Sea is illustrated in Figure 3. In Figure 15, the mean annual salinity for DSOW in the Labrador Sea (cyan symbols) is compared to the time series of mean salinities for DSOW on Line W (blue symbols). The mean salinities were calculated in both cases by averaging values for the same set of samples used to estimate the ^{129}I and CFC-11 time series shown in Figure 9. The Labrador Sea salinity time series was approximated by a sine curve having a period of 5 years and amplitude of 0.27 (solid dark pink curve in Figure 15). This periodic signal is used as the input for the boundary current model using parameter values; $t_{adv} =$ 6 years; $t_{mix} =$ 3 years; $\alpha = 0.25$ to give the upper dashed curve in Figure 15. These parameter values give the resulting periodic signal a phase lag of 6 years and amplitude equal to 0.2 times the amplitude of the tracer signal in the Labrador Sea. In this case a constant positive salinity offset of 0.02 has been applied to the model results in order to compare them to the Line W results. The salinity offset is assumed to occur through mixing of DSOW with higher salinity AABW having negligible tracer concentrations. The fit of the model results for the Labrador Sea salinity input signal (sine wave of period 5 years) to the Line W salinities can be characterized by the root mean squares (RMS) of the differences between model and experimental results. These results are illustrated in Figure 16 (middle) where the RMS errors are plotted as a function of parameter values for t_{adv} and t_{mix} ($\alpha = 0.25$). Troughs in the t_{adv} versus t_{mix} RMS surface representing the best fits to the Line W results occur for values of $t_{adv} = 3$, 8.5, and 13 years, corresponding to advection velocities of 4.9, 1.7, and 1.1 cm/s, respectively. However, the lowest RMS values occur for $t_{mix} \leq 1$ year. High rates of mixing tend to diminish the amplitude of the periodic signal resulting in a dampened salinity curve that represents an improved fit to the Line W results. Similar results are obtained by using the actual Labrador Sea salinity data [*Yashayaev*, 2007; *Yashayaev et al*., 2007] without invoking the sine curve approximation and calculating the phase shift and amplitude following *Waugh and Hall* [2005].

The RMS distributions for the ^{129}I and CFC-11 results (Figures 12 and 13, bottom) were normalized to values for their respective ranges and combined to give a single normalized RMS (NRMS) distribution for the tracer core and interior (Figure 16, top). These results were then combined with the RMS distribution for salinity (Figure 16, middle) also normalized to its range to give the combined NRMS distribution in Figure 16 (bottom). The lowest values of the NRMS calculated for $\alpha = 0.25$ lie in the same ranges of parameter values ($t_{adv} =$ 5–6 years; $t_{mix} =$ 2–4 years) as those determined from the ^{129}I – CFC-11 analysis alone. The inclusion of the salinity time series in the RMS analysis decreases the resolution of the contour minima in the RMS plot for t_{adv} and t_{mix} and skews the broad minima toward greater values of t_{adv} and t_{mix}, but does not alter the optimum model parameter values. Generally, the data-model comparisons for the hydrographic analysis are not very useful in further constraining model parameters, but they are included for completeness.

4.8. Comparison With Other Studies

van Sebille et al. [2011] compared the temporal variability in hydrographic properties of CLSW observed on the AR7W line in the Labrador Sea with those measured on the Abaco Line at 26°N near the Bahamas. A transport time of 9 years, corresponding to a mean flow velocity of 2.5 cm/s, was determined by maximizing the correlations of salinity time series at both locations, a result that is in agreement with earlier studies [*Molinari et al*., 1998]. They used the high resolution, numerical model, OFES to determine hydrographic time series at node points on DWBC flow pathways close to the continental shelf and on interior pathways

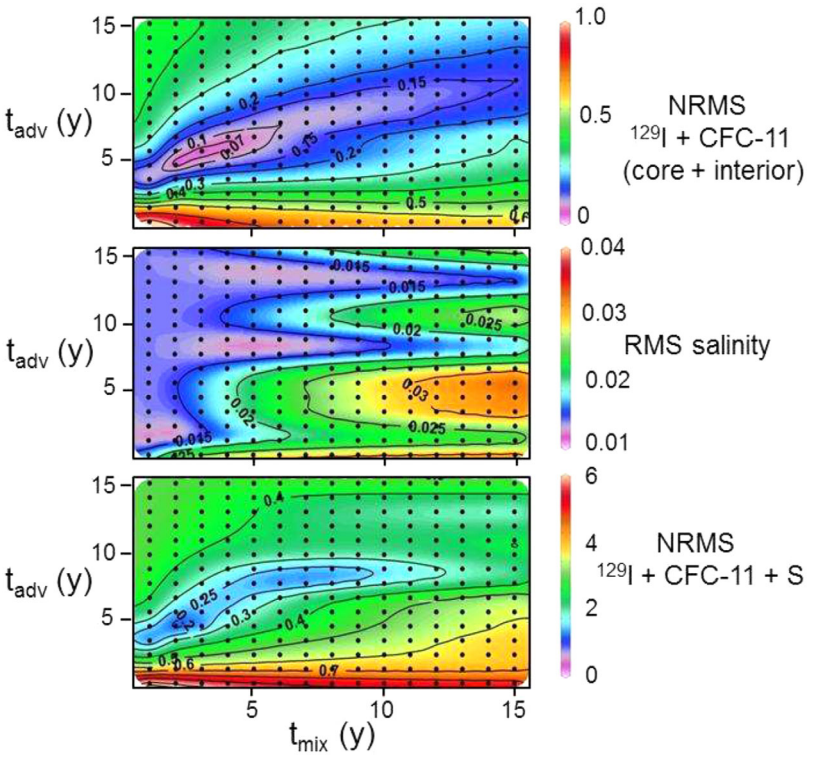

Figure 16. (top) Contoured plots of NRMS errors for t_{adv} versus t_{mix} ($\alpha = 0.25$) for CFC-11 (core + interior) and ^{129}I (core + interior) combined. (middle) RMS errors for fit of model salinity results to core Line W time series results as illustrated in Figure 15. The troughs in the t_{adv} versus t_{mix} RMS surface occur for values of t_{adv} = 3, 8, and 13 years. (bottom) Contoured plots combined for NRMS for CFC-11 (core + interior), ^{129}I (core + interior) and core salinity from middle panel. The combined NRMS results have the minima range (t_{adv} = 5–6 years; t_{mix} = 2–3 years) consistent with the ^{129}I and CFC-11 RMS separately.

in the Atlantic basin. Comparisons of the OFES results with the Labrador Sea and Abaco time series shows a discontinuity in flow velocities along the DWBC path near the tail of the Grand Banks with flow time scales from the Labrador Sea to the southeastern Grand Banks of 1–3 years increasing abruptly to 7–9 years over the southwestern Grand Banks. These simulations were consistent with the results of *Bower et al*. [2009, 2011], as noted above, that showed separation of the boundary current from the slope near the tail of the Grand Banks and the establishment of interior flow pathways. *Lozier et al*. [2013] extended these studies of LSW to the overflows (OW) using an ocean general circulation model and also observed that recirculations promote a significant amount of equatorward flow of OW by interior pathways rather than in the DWBC.

In a more recent study, *Rhein et al*. [2015] applied the TTD methodology based on 1-D inverse Gaussian distributions [*Waugh et al*., 2004] to a compilation of CFC data collected over a 25 years period in the North Atlantic Ocean. Both mixing and advection are included in the 1-D Gaussian distribution, but these terms are for an undefined pathway between the source regions and the point of observation. Lateral mixing between the DWBC and the interior is not explicitly included in their formulation. The difference between mean tracer ages for water less than 40 years old for the DSOW density horizon in the Labrador Sea (8 years) and at Line W (19 years) determined by *Rhein et al*. [2015] was 11 years which can be compared to the advection time, t_{adv} of 5–6 years calculated using the boundary current model in the present study. This does not necessarily represent a disagreement, because mean tracer ages determined from the TTD methodology will always be greater than advection times calculated using the boundary current model. The tracer age includes the effects of mixing and will decrease to approach the value of the advection time as the degree of mixing is reduced. Mixing and advection are separately parameterized in the boundary current model while in the *Rhein et al*. [2015] application an assumption must be made about their relative values.

Andres et al. [2016] have also used CFC measurements from Line W to investigate lateral exchange of DSOW between the DWBC and interior regimes. The age (time since the water departed the source region north of Denmark Strait) of the DSOW core of the DWBC was calculated from CFC-11:CFC-12 and CFC-113:CFC-12

ratios, yielding 13 ± 5 and 23 ± 5 years, respectively. This difference was inferred to stem from the effect of mixing on the ratio ages and was cited as evidence showing the importance of the boundary current core and interior exchange processes that are outlined in detail in the present study.

4.9. Advection and Mixing Times

The boundary current model parameters and circulation pathways for DSOW flow in the DWBC and through the interior are outlined in Figure 17. The ranges of parameter values for DSOW flow in the DWBC from the Labrador Sea to Line W based on the combination of tracers of ^{129}I, CFC-11, and salinity and $\alpha = 0.25$ are t_{adv} = 5–6 years (u = 2.4–2.9 cm/s); t_{mix} = 2–4 years while the ^{129}I analysis alone based on an exponential fit to the ^{129}I Labrador Sea input function gives a value of t_{adv} = 5.4 years (u = 2.7 cm/s); t_{mix} = 2.6 years. Typically, current velocities in the core of the DWBC measured on Line W using both shipboard profiling data and moored arrays [*Toole et al*., 2011] are about 5 cm/s, almost twice the mean flow velocity of 2.7 cm/s estimated in the present study. However, the present results represent decadal means over the broad range of flow and mixing pathways between the Labrador Sea and Line W and do not necessarily represent the specific conditions prevailing on Line W at the time of sampling. *Rhein et al*. [2015] identified a slowing of the DSOW component of the DWBC in the subpolar/subtropical transition zone upstream of Line W proximal to the Newfoundland Basin and the tail of the Grand Banks. Strong interaction occurs between the DWBC and the northward flowing NAC in this region leading to the incorporation of older, deep water into the DWBC. Upstream slowing of the DWBC, also noted by *van Sebille et al*. [2011] for LSW, would be reflected at downstream locations by lower flow velocities and higher mixing rates compared to ambient conditions in applications of the boundary current model. The mixing undergone by the DWBC is predominantly isopycnal, but also includes some diapycnal mixing between DSOW and overlying ISOW, particularly in the subpolar basin. Mixing between DSOW core and interior waters may be enhanced during Gulf Stream meandering and the formation of troughs that promote deep cyclogenesis. *Andres et al*. [2016] have indicated that cyclone-driven stirring and mixing on Line W can enhance core-interior tracer exchange on short time scales (weeks to months) and affect both the position of the core and the value of the boundary current model parameter, α.

Interior pathways contributing to the flow of DSOW over the Bermuda Rise are illustrated schematically by dashed curves in Figure 17. The remarkably well-defined tracer cores observed on the Dynamite Line may partially stem from northeastward recirculation of DWBC from the Gulf Stream mixing region (solid arrows in Figure 17) and subsequent deflection southward (dashed line) at the New England Seamounts, whose presence acts as a barrier and influences circulation at depths below 3500 m. This could generate a boundary current steered to the southwest around the Bermuda Rise that would be more coherent than would be expected from the less topographically constrained flow through the interior. Elevated tracer levels observed in the interior region at the southern end of Line W in several years (particularly in 2013 and 2014; Figure 5) may also be influenced by the anticyclonic recirculation around Bermuda (dotted lines in Figure 17) of the interior DSOW flow across the Dynamite Line [*Andres et al*., 2016] followed by northeastward flow across Line W.

5. Conclusions

Time series tracer measurements of ^{129}I and CFC-11 in DSOW were carried out in the DWBC on Line W during 2004–2014 and compared to upstream time series tracer measurements in DSOW in the Labrador Sea (1993–2014) to determine flow properties in the DWBC. The Labrador Sea tracer results were used as input functions in boundary current model simulations of downstream tracer concentrations in core and interior regions of the DWBC at Line W. The ratio, α, of the width of the boundary current core to that of the interior shoulder region with which tracer mixing occurs was estimated to have a value of 0.25 based on the configuration of CFC-11 sections. Model results indicate that the advection time, t_{adv} for DSOW between the Labrador Sea and Line W is 5–6 years, corresponding to a mean advection flow velocity, u of 2.4–2.9 cm/s. Mixing between the core of the boundary current and the interior shoulder region occurs with a time constant, t_{mix} of 2–4 years. ^{129}I measurements, alone gave analytical solutions using the boundary current model of t_{adv} = 5.4 years (u = 2.7 cm/s); t_{mix} = 2.6 years based on an exponential fit to the ^{129}I input function in the Labrador Sea. Tracer measurements conducted over the Bermuda Rise, southeast of Bermuda showed the presence of a core of DSOW flowing equatorward through the western basin of the North Atlantic by

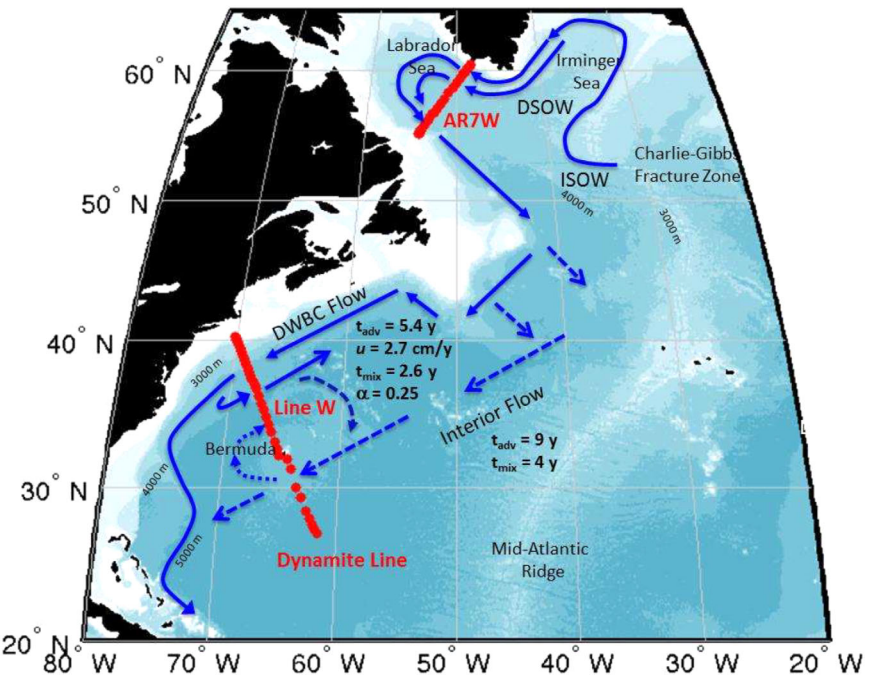

Figure 17. Schematic of flow pathways discussed in the text. Boundary current model with $\alpha = 0.25$ gives parameter values for exponential ^{129}I input function of $t_{adv} = 5.4$ years ($u = 2.7$ cm/s), $t_{mix} = 2.6$ years for flow of DSOW in the DWBC (solid arrows) and $t_{adv} = 9$ years, $t_{mix} = 4$ years for interior flow (dashed arrows). Both recirculation from DWBC (solid arrows) and interior flow can contribute to tracer transport across Dynamite Line. Anticyclonic recirculation of interior flow of DSOW northeastward around Bermuda is illustrated by dotted arrows.

interior pathways as predicted by model simulations and float studies [*Lozier et al.*, 2013]. Model parameter values estimated for core DSOW over the Bermuda Rise based on a single tracer section in 2010 are $t_{adv} = 9$ years; $t_{mix} = 4$ years. The present study shows that measurements of the tracer distributions in both the core and interior regions, between which mixing occurs are essential to the realization of the full potential of the *Waugh and Hall* [2005] boundary current model.

Acknowledgments

The authors wish to express their thanks to the scientific staff, officers, and crews of the many US and Canadian vessels engaged in carrying out this work. We also thank J. Loder, P. Rhines, and D. Waugh for their reviews and helpful comments. The BIO hydrographic (CTD) shifts performed the tracer sample collection in the Labrador Sea. R. Nelson and G. Folwarczna undertook much of the ^{129}I sample collection and analyses at BIO, E. Gorman made most of the Line W CFC measurements, H. Lee undertook data reduction and analysis, J. Happel made the CFC measurements on the 2010 Line W cruise and the US NSF supported this work through the following grants: OCE-0241354, OCE-0726720, OCE-0926848, and OCE13-32834. Labrador Sea data can be accessed through: http://www.bio.gc.ca/science/monitoring-monitorage/azomp-pmzao/labrador/labrador-en.php and Line W data can be downloaded from http://www.whoi.edu/science/PO/linew/download_data.php.

References

Andres, M., J. M. Toole, D. Torres, W. M. Smethie Jr., T. M. Joyce, and R. G. Curry (2016), Stirring by deep cyclones and the evolution of Denmark Strait Overflow Water observed at Line W, *Deep Sea Res., Part I*, *109*, 10–26, doi:10.1016/j.dsr2015.12.011.

Azetsu-Scott, K., E. P. Jones, I. Yashayaev, and R. M. Gershey (2003), Time series study of CFC concentrations in the Labrador Sea during deep and shallow convection regimes (1991-2000), *J. Geophys. Res.*, *108*(C11), 3354, doi:10.1029/2002JC001317.

Azetsu-Scott, K., E. P. Jones, and R. M. Gershey (2005), Distribution and ventilation of water masses in the Labrador Sea inferred from CFCs and carbon tetrachloride, *Mar. Chem.*, *94*, 55–66.

Bower, A. S., and H. D. Hunt (2000a), Lagrangian observations of the deep western boundary current in the North Atlantic Ocean Part I: Large-scale pathways and spreading rates, *J. Phys. Oceanogr.*, *30*, 764–783.

Bower, A. S., and H. D. Hunt (2000b), Lagrangian observations of the deep western boundary current in the North Atlantic Ocean Part II: The Gulf Stream-deep western boundary crossover, *J. Phys. Oceanogr.*, *30*, 784–804.

Bower, A. S., M. S. Lozier, S. F. Gary, and C. Böning (2009), Interior pathways of the Atlantic meridional overturning circulation, *Nature*, *459*, 243–247, doi:10.1038/nature07979.

Bower, A. S., M. S. Lozier, and S. F. Gary (2011), The export of Labrador Sea Water from the subpolar North Atlantic: A Lagrangian perspective, *Deep Sea Res., Part II*, *58*, 1798–1818.

Curry, R. G., M. S. McCartney, and T. M. Joyce (1998), Oceanic transport of subpolar climate signals to mid-depth subtropical waters, *Nature*, *391*, 575–577, doi:10.1038/35356.

Dickson, B., I. Yashayaev, J. Meincke, B. Turrell, S. Dye, and J. Holfort (2002), Rapid freshening of the deep North Atlantic Ocean over the past four decades, *Nature*, *416*, 832–837.

Doney, S. C., and W. J. Jenkins (1994), Ventilation of the deep western boundary current and abyssal western North Atlantic: Estimates from tritium and ^{3}He distributions, *J. Phys. Oceanogr.*, *24*, 638–659.

Edmonds, H. N., J. N. Smith, L. R. Kilius, H. D. Livingston, and J. M. Edmond (1998), ^{129}I in archived seawater samples: Source functions and tracer comparisons, *Deep Sea Res., Part I*, *45*(6), 1111–1125.

Edmonds, H. N., Z. Q. Zhou, G. M. Raisbeck, F. Yiou, L. Kilius, and J. M. Edmond (2001), Distribution and behaviour of anthropogenic ^{129}I in water masses ventilating the North Atlantic Ocean, *J. Geophys. Res.*, *106*(C4), 6881–6894.

Fine, R. A., M. Rhein, and A. Chantal (2002), Using a CFC effective age to estimate propagation and storage of climate anomalies in the deep western North Atlantic Ocean, *Geophys. Res. Lett.*, *29*(24), 2227, doi:10.1029/2002GL015618.

Fischer, J., F. A. Schott, and M. Dengler (2004), Boundary circulation at the exit of the Labrador Sea, *J. Phys. Oceanogr.*, *34*, 1548–1570.

Fogelqvist, E., J. Blindheim, T. T. Tanhua, S. Osterhus, E. Buch, and F. Rey (2003), Greenland-Scotland overflow studied by hydro-chemical multivariate analysis, *Deep Sea Res., Part I*, *50*, 73–102.
Freudenthal, S., and C. Andrie (2002), The arrival of a ''new'' Labrador Sea Water signal in the tropical Atlantic in 1996, *Geophys. Res. Lett.*, *29*(15), 1741, doi:10.1029/2002GL015062.
Gary, S. F., M. S. Lozier, C. Böning, and A. Biastoch (2011), Deciphering the pathways for the deep limb of the meridional overturning circulation, *Deep Sea Res., Part II*, *58*, 1781–1797.
Greenan, B., G. Harrison, I. Yashayaev, K. Azetsu-Scott, E. Head, W. Li, and J. Loder (2010), Physical, chemical and biological conditions in the Labrador Sea in 2009, *AZMP Bull.*, *9*, 11–19.
Haine, T. W. N., A. J. Watson, M. I. Liddicoat, and R. R. Dickson (1998), The flow of Antarctic bottom water to the southwest Indian Ocean estimated using CFCs, *J. Geophys. Res.*, *103*(C12), 27,637–27,653.
Hogg, N. G., R. S. Pickart, R. M. Hendry, and W. M. Smethie Jr. (1986), The northern recirculation gyre of the Gulf Stream, *Deep Sea Res., Part A*, *33*, 1139–1165.
IPCC (2014), *Climate Change 2014: Synthesis Report. Contribution of Working Groups 1, II and III to the Fifth Assessment Report of the Intergovernmental Panel on Climate Change*, 151 pp., Geneva, Switzerland.
Kilius, L., A. E. Litherland, J. C. Rucklidge, and N. Baba (1992), Accelerator mass spectrometric measurements of heavy long-lived isotopes, *J. Appl. Radiat. Isot.*, *43*, 279–287.
Kilius, L. R., J. C. Rucklidge, and C. Soto (1994), The dispersal of ^{129}I from the Columbia River estuary, *Nucl. Instrum. Methods*, *B92*, 393–397.
LeBel, D. A., W. M. Smethie Jr., M. Rhein, D. Kieke, R. A. Fine, J. L. Bullister, D.-H., Min, W. Roether, R. F. Weiss, A. Chantal, D. Smythe-Wright, and E. P. Jones (2008), The distribution of CFC-11 in the North Atlantic during WOCE: Inventories and calculated water mass formation rates, *Deep Sea Res., Part I*, *55*, 891–910.
Lozier, M. S., S. F. Gary, and A. Bower (2013), Simulated pathways of the overflow aters in the NorthAtlantic: Subpolar to subtropical export, *Deep Sea Res., Part II*, *85*, 147–153.
Mauldin, A., P. Schlosser, R. Newton, W. M. Smethie Jr., R. Bayer, M. Rhein, and E. P. Jones (2010), The velocity and mixing time scale of the Arctic Ocean Boundary Current estimated with transient tracers, *J. Geophys. Res.*, *115*, C08002, doi:10.1029/2009JC005965.
Mauritzen, C. (1996), Production of dense overflow waters feeding the North Atlantic across the Greenland-Scotland Ridge, part I: Evidence for a revised circulation scheme, *Deep Sea Res., Part I*, *43*, 769–806.
Molinari, R. L., R. A. Fine, W. D. Wilson, R. G. Curry, J. Abell, and M. S. McCartney (1998), The arrival of recently formed Labrador Sea Water in the deep western boundary current at 26.5°N, *Geophys. Res. Lett.*, *25*(13), 2249–2252.
Pēna-Molino, B., T. M. Joyce, and J. M. Toole (2011), Recent changes in the Labrador Sea Water within the Deep Western Boundary Current southeast of Cape Cod, *Deep Sea Res., Part II*, *58*(10), 1019–1030, doi:10.1016/j.dsr.2011.07.006.
Pickart, R. S., and W. M. Smethie Jr. (1993), How does the Deep Western Boundary Current cross the Gulf Stream?, *J. Phys. Oceanogr.*, *23*, 2602–2616.
Pickart, R. S., and W. M. Smethie (1998), Temporal evolution of the deep western boundary current where it enters the subtropical domain, *Deep Sea Res., Part A*, *45*, 1053–1083.
Pickart, R. S., N. G. Hogg, and W. M. Smethie (1989), Determining the strength of the Deep Western Boundary Current using the chlorofluoromethane ratio, *J. Phys. Oceanogr.*, *19*, 940–951.
Rhein, M. (1994), The deep western boundary current—Tracers and velocities, *Deep Sea Res., Part A*, *41*, 263–281.
Rhein, M., D. Kieke, and R. Steinfeldt (2015), Advection of North Atlantic Deep Water from the Labrador Sea to the southern hemisphere, *J. Geophys. Res. Oceans*, *120*, 2471–2487, doi:10.1002/2014JC010605.
Rudels, B., P. Eriksson, H. Grönvall, R. Hietala, and J. Launiainen (1999), Hydrographic observations in Denmark Strait in Fall 1997, and their implications for the entrainment into the overflow plume, *Geophys. Res. Lett.*, *26*(9), 1325–1328.
Rudels, B., U. Schauer, G. Bjork, M. Korhonen, S. Pisarev, and A. Wisotzki (2013), Observations of water masses and circulation with focus on the Eurasian Basin of the Arctic Ocean from the 1990s to the late 2000s, *Ocean Sci.*, *9*, 147–169.
Smethie, W. M., Jr. (1993), Tracing the thermalhaline circulation in the western North Atlantic using chlorofluorcarbons, *Prog. Oceanogr.*, *31*, 51–99.
Smethie, W. M., Jr., and R. A. Fine (2001), Rates of North Atlantic Deep Water formation calculated from chlorofluorocarbon inventories, *Deep Sea Res., Part A*, *48*, 189–215.
Smethie, W. M., Jr., and J. H. Swift (1989), The tritium: Krypton-85 age of Denmark Strait overflow water and Gibbs fracture zone water just south of Denmark Strait, *J. Geophys. Res.*, *94*, 8265–8275.
Smethie, W. M., Jr., R. A. Fine, A. Putzka, and E. P. Jones (2000), Tracing the flow of North Atlantic Deep Water using chlorofluorocarbons, *J. Geophys. Res.*, *105*, 14,297–14,323.
Smith, J. N., K. M. Ellis, and L. R. Kilius (1998), ^{129}I and ^{137}Cs tracer measurements in the Arctic Ocean, *Deep Sea Res., Part I*, *45*, 959–984.
Smith, J. N., K. M. Ellis, and T. M. Boyd (1999), Circulation features in the Central Arctic Ocean revealed by nuclear fuel reprocessing tracers from SCICEX 95 and 96, *J. Geophys. Res.*, *104*(C12), 29,663–29,677.
Smith, J. N., E. P. Jones, S. B. Moran, W. M. Smethie Jr., and W. E. Kieser (2005), ^{129}I/CFC-11 transit times for Denmark Strait Overflow Water in the Labrador and Irminger Seas, *J. Geophys. Res.*, *110*, C05006, doi:10.1029/2004JC002516.
Smith, J. N., F. A. McLaughlin, W. M. Smethie Jr., S. B. Moran, and K. Lepore (2011), Iodine-129, ^{137}Cs, and CFC-11 tracer transit time distributions in the Arctic Ocean, *J. Geophys. Res.*, *116*, C04024, doi:10.1029/2010JC006471.
Steinfeldt, R., M. Rhein, and M. Walter (2007), NADW transformation at the western boundary between 66°W/20°N and 60°W/10°N, *Deep Sea Res., Part I*, *54*(6), 835–855.
Stommel, H. (1958), The abyssal circulation, *Deep Sea Res.*, *5*, 80–82.
Swift, J. H. (1984), The circulation of the Denmark Strait and Iceland-Scotland overflow waters in the North Atlantic, *Deep-Sea Res., Part A*, *31*, 1339–1355.
Swift, J. H., K. Aagaard, and S. V. Malmberg (1980), The contribution of the Denmark Strait Overflow to the deep North Atlantic, *Deep Sea Res., Part A*, *27*, 29–42.
Toole, J. M., R. G. Curry, T. M. Joyce, M. McCartney, and B. Peña-Molino (2011), Transport of the North Atlantic Deep Western Boundary Current about 39°N, 70°W: 2004–2008, *Deep Sea Res., Part II*, *58*, 1768–1780.
Våge, V. K., R. S. Pickart, M. A. Spall, H. Valdimarsson, S. Jónsson, D. J. Torres, S. Østerhus, and T. Eldevik (2011), Significant role of the North Icelandic Jet in the formation of Denmark Strait overflow water, *Nat. Geosci.*, *4*, 723–727.
Våge, V. K., R. S. Pickart, M. A. Spall, G. W. K. Moore, H. Valdimarsson, D. J. Torres, S. Y. Erofeeva, and J. E. Ø. Nilsen (2013), Revised circulation scheme north of the Denmark Strait, *Deep Sea Res., Part 1*, 79, 20–39.

van Sebille, E., M. O. Baringer, W. E. Johns, C. S. Meinen, L. M. Beal, M. F. de Jong, and H. M. van Aken (2011), Propagation pathways of classical Labrador Sea water from its source region to 26°N, *J. Geophys. Res.*, *116*, C12027, doi:10.1029/2011JC007171.

Watts, D. R. (1991), Equatorward currents in temperatures 1.8–6.0°C on the continental slope in the Mid-Atlantic Bight, in *Deep Convection and Deep Water Formation in the Oceans*, edited by P. C. Chu and J. C. Gascard, pp. 183–196, Elsevier, Amsterdam.

Waugh, D. W., and T. M. Hall (2005), Propagation of tracer signals in boundary currents, *J. Phys. Oceanogr.*, *35*, 1538–1552, doi:10.1175/JPO2779.1.

Waugh, D. W., T. W. N. Haine, and T. M. Hall (2004), Transport times and anthropogenic carbon in the subpolar North Atlantic Ocean, *Deep Sea Res., Part I*, *51*(11), 1475–1491.

Xu, X., P. B. Rhines, E. P. Chassignet, and W. J. Schmitz Jr. (2015), Spreading of Denmark Strait overflow water in the western subpolar North Atlantic: Insights from eddy-resolving simulations with a passive tracer, *J. Phys. Oceangr.*, *45*, 2913–2932, doi:10.1175/JPO-D-14-0179.1.

Yashayaev, I. (2007), Hydrographic changes in the Labrador Sea, 1960–2005, *Prog. Oceanogr.*, *73*, 242–276, doi:10.1016/j.pocean.2007.04.015.

Yashayaev, I., and R. R. Dickson (2008), Transformation and fate of overflows in the northern North Atlantic, in *Arctic-Subarctic Ocean Fluxes: Defining the Role of the Northern Seas in Climate*, edited by R. R. Dickson, J. Meincke, and P. Rhines, pp. 505–526, Springer, Dordrecht, Netherlands.

Yashayaev, I., H. M. Van Aken, N. P. Holliday, and M. Bersch (2007), Transformation of the Labrador Sea Water in the subpolar North Atlantic, *Geophys. Res. Lett.*, *34*, L22605, doi:10.1029/2007GL031812.

Zhang, R. (2010), Latitudinal dependence of Atlantic meridional overturning circulation (AMOC) variations, *Geophys. Res. Lett.*, *37*, LI6703, doi:10.1029/2010GL044474.